

AD-A053 442

AIR FORCE INST OF TECH WRIGHT-PATTERSON AFB OHIO SCH--ETC F/G 4/1
ATMOSPHERIC ATTENUATION OF HENE LASER RADIATION.(U)
DEC 77 6 6 WILLIFORD

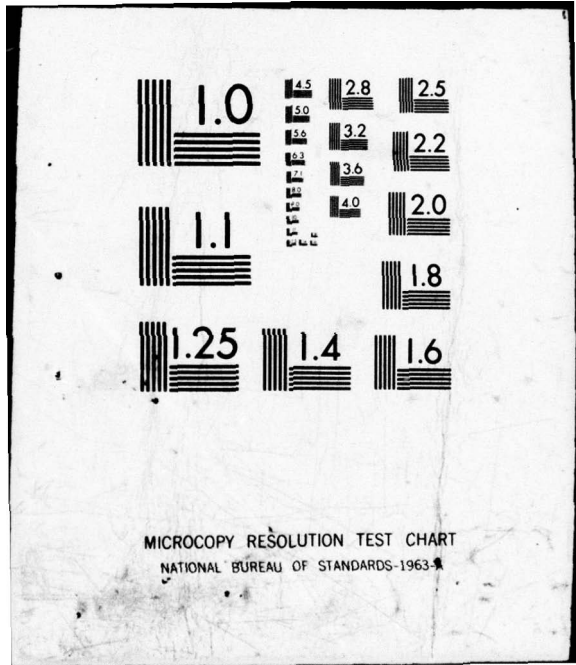
UNCLASSIFIED

AFIT/GEP/PH/77-17

NL

1 OF 1
AD
A063442

END
DATE
FILMED
6-78
DDC



MICROCOPY RESOLUTION TEST CHART
NATIONAL BUREAU OF STANDARDS-1963-A

AD No.
 DDC FILE COPY

AD A 053442

①

DDC
MAY 2 1978
W.F.

ATMOSPHERIC ATTENUATION OF
HeNe LASER RADIATION

THESIS

GEP/PH/77-17 ✓ Graham G. Williford
Captain USAF

6 ATMOSPHERIC ATTENUATION OF
HeNe LASER RADIATION •

9 Master's THESIS,

Presented to the Faculty of the School of Engineering
of the Air Force Institute of Technology
Air University
in Partial Fulfillment of the
Requirements for the Degree of
Master of Science

14 AFIT/GEP/PH/77-17
by 12 77p.

7φ Graham G. Williford
~~████████████████████~~

Graduate Engineering Physics

11 Dec ██████████ 77

Approved for public release; distribution unlimited

ACCESSION for	
NTIS	White Section <input checked="" type="checkbox"/>
DDC	Buff Section <input type="checkbox"/>
UNANNOUNCED	<input type="checkbox"/>
JUSTIFICATION	
FY	
DISTRIBUTION/AVAILABILITY CODES	
SPECIAL	
A	

φ12 225-

2

Preface

The purpose of this research was to establish an optical range and use it to study atmospheric attenuation of laser radiation. Initial testing was done with a HeNe laser. Follow-on testing, which is being planned by the Air Force Avionics Laboratory, will be conducted with various other lasers, including a CO₂ laser. A delay was encountered awaiting safety approval for the project, and experimentation time was limited to the last four weeks at the end of the period available for research. For this reason the amount of experimental data is limited. Fortunately, during the time which was available for testing a large variety of weather conditions could be observed, and useful information could be extracted from the data.

I am very grateful to my thesis advisor, Major Bruce Pierce, for all the help and encouragement he gave me throughout the project. Without his help the project could not have been completed. To the technicians in the physics department, whose assistance I required on numerous occasions, I owe my thanks. In addition, I want to thank my sponsor, Mr. Vince Chemilis, for the excellent technical advise and material support which he provided.

Finally, I owe the most to my wife, Susan, for her endless encouragement, understanding, and love.

Graham G. Williford
Captain, USAF

Contents

Preface	ii
List of Figures	v
List of Tables	vi
Abstract	vii
I. Introduction	1
II. Theory	8
Atmospheric Attenuation	8
Molecular Scattering	9
Molecular Absorption	9
Aerosol Attenuation	13
Effects of Atmospheric Turbulence	16
Spot Dancing	17
Beam Spreading	19
Image Dancing	21
Scintillation	21
III. Equipment	26
Transmitting Equipment	26
HeNe Laser	26
Beam Expanding Telescope	28
Table Mount	30
Safety Pipe	30
Receiving Equipment	31
Mirror	31
Detector	31
XY Recorder	33
Additional Equipment	34
Beam Splitter	34
Detection Equipment Used with Beam Splitter	35
#2 HeNe Laser	35
IV. Experimental Design and Operation	36
Laboratory Testing	36
Telescope Alignment	36
Test of Laser Stability	37
Classification of Optics	38
Comparison of #1 and #2 Lasers	38
Field Calibrations	38
A Range Description	39
Equipment Alignment	42
Field of View Adjustment	42
Nighttime Alignment	42

Daytime Alignment	45
Beam Drift	45
Test Run Procedures	46
Warmup Period	46
Recalibration	46
Realignment	47
Weather Observations	47
Transmission Measurement	47
 V. Experimental Results and Data Analysis	 49
Transmission Measurements	49
Turbulence Effects	52
Spot Dancing	52
Beam Spreading	52
Image Dancing	53
Scintillation	53
 VI. Conclusions and Recommendations	 54
Conclusions	54
Recommendations	55
Concurrent Testing	55
Visibility Measurements	55
Future Test Approval	55
Joint Research Project	56
 Bibliography	 57
Appendix A: Standard Operating Procedures (SOP) for Outdoor Testing of Open-Air Lasers	59
Appendix B: Radiation Hazard Evaluation For HeNe Laser . .	63
Appendix C: Radiation Hazard Evaluations For CO ₂ Lasers . .	64
Appendix D: Error Analysis for Experimental Results	65
Vita	66

List of Figures

Figure	Page
1 General Range Diagram	2
2 Theoretical Transmission versus Visibility for HeNe Laser	15
3 Diurnal Variation of CO ₂ Laser Spot Characteristics	17
4 Effect of Index of Refraction Change	19
5 Intensity Distribution of Focused Laser at 0.63 um	24
6 Intensity Distribution of Focused Laser at 10.6 um	25
7 Safety Pipe Mounted on Rail of Bldg 620 Tower Balcony	27
8 Transmitter- Laser and Support	27
9 Collimating Telescope	29
10 Power Measuring Equipment	32
11 Target Mirror	32
12 Overhead Diagram of Range	40
13 Vertical Diagram of Range	41
14 View of Bldg 22B Penthouse from Bldg 620 Tower	43
15 View of Bldg 620 Tower from Bldg 22B Penthouse	43
16 Blowup of Fig. 15 Showing Maximum Field of View	44
17 Visible Range of Prominent Local Features As Viewed From the Tower of Bldg 620	48
18 Comparison of Experimental and Theoretical Results for HeNe Laser (Percent Transmission versus Visibility)	51

List of Tables

Table		Page
I	Attenuation Coefficients for HeNe Laser	10
II	Attenuation Coefficients for Nd:YAG Laser	11
III	Attenuation Coefficients for CO ₂ Laser	12
IV	Test Run Data	50

Abstract

Atmospheric attenuation of a low-power HeNe laser beam was examined both theoretically and experimentally. Experimental results were limited, but useful information could be extracted from the data. Close agreement was found between experimental results and theoretical predictions based on interpolation between aerosol coefficients given by McClatchey and Selby.

The effects of atmospheric turbulence upon laser propagation were also examined. An attempt was made to minimize the effect turbulence had upon test results, so that atmospheric attenuation could be studied independently. The conclusion of a theoretical study was that this could be accomplished by using a receiver several times larger than the beam size at the target. The prediction proved true during test runs.

The experimentation was conducted over a 1.23 kilometer course, using a 2 milliwatt HeNe laser as the transmitter, and a 12 inch spherical mirror as the receiver. Tests were conducted under visibility conditions ranging from 2 kilometers to 18 kilometers.

ATMOSPHERIC ATTENUATION OF
HeNe LASER RADIATION

I. Introduction

Low powered lasers are used by the Air Force as sources of illumination in targeting systems. Utilizing this laser-guidance, under optimum conditions weapons can be delivered with extreme accuracy. Experience has shown, however, that the effective range of such weapons is strongly dependent upon weather conditions and the type of laser in use. Bad weather, in particular low visibility, can make certain of these systems unusable. Other lasers, such as the CO₂ laser, may be little affected by reduced visibility. Because the amount of atmospheric attenuation varies by laser type, the need exists to study several lasers under a variety of well-documented weather conditions. A laser range, to be utilized for that purpose, was established at Wright Patterson AFB, Ohio. Final results from experiments conducted on the range may be of significant value in the selection of suitable lasers for future targeting systems. In addition, knowledge of the atmospheric limitations of a specific laser system, will be of great importance during operational planning involving utilization of that system.

Establishment of the laser range and its initial operation are the subjects of this report. Using existing equipment and facilities, developmental planning and first stage operation of the range was accomplished. A general diagram of the laser range follows in Figure 1.

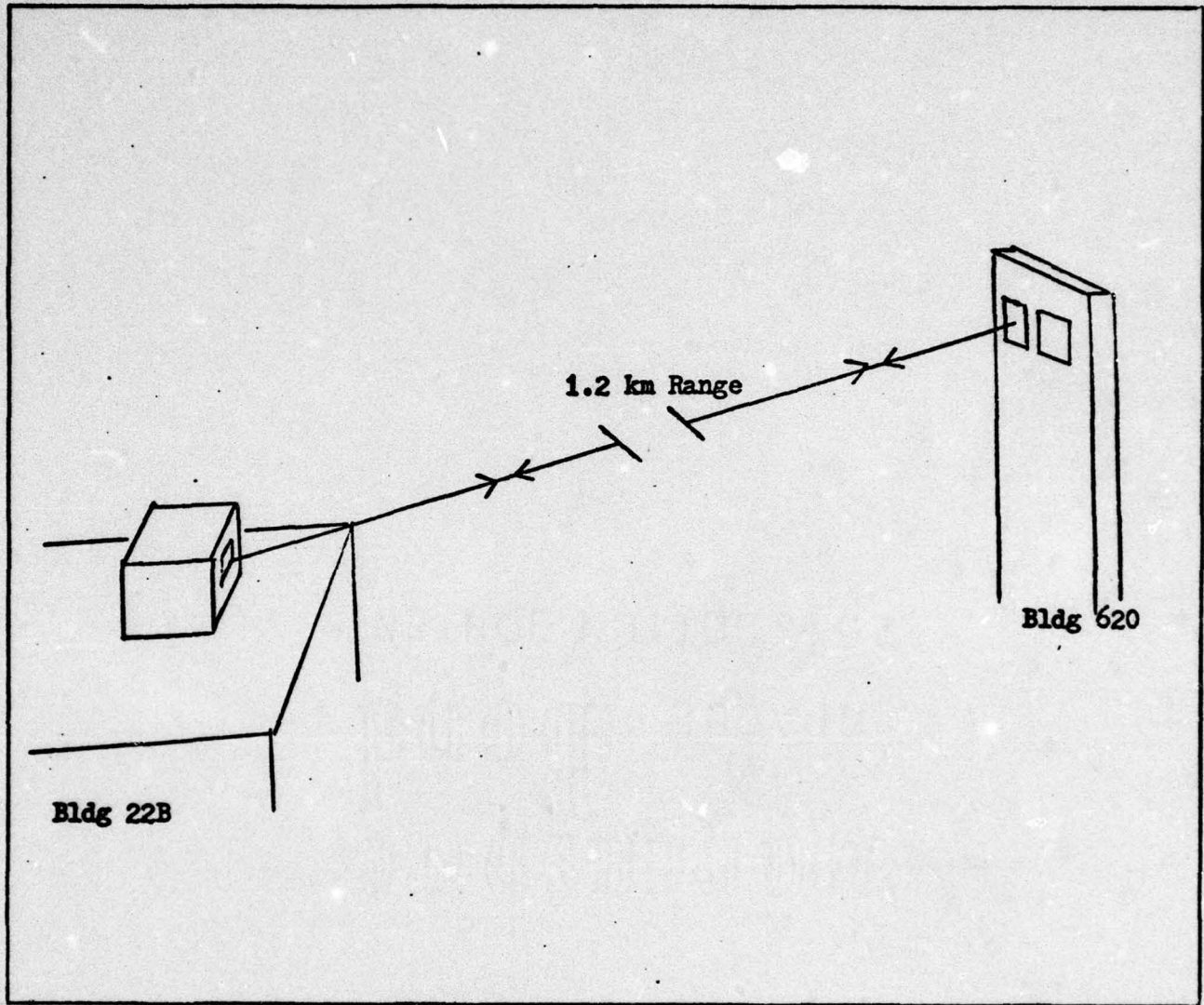


Fig. 1. General Range Diagram

As is noted in the diagram, the optical path extended over a 1.2 kilometer path from the tower of Building 620 to the penthouse of Building 22B. The original plan was to begin testing with a CO₂ laser. Unfortunately, the CO₂ laser, which was to be used, was broken during shipment. Also, it became apparent that a long delay would be encountered awaiting safety approval for the use of a CO₂ laser. For these reasons, the decision was made to use a HeNe laser during initial range operation. The HeNe laser was chosen because of its availability, safety, and ease of operation. This laser is not a candidate for use in future targeting systems, but it will be used in later tests for alignment purposes and as a reference of atmospheric attenuation in the visible portion of the spectrum. The CO₂ laser will be the first strong candidate for use in a laser-guidance weapon system which will undergo follow-on testing.

Prior to actual testing, several procedural steps of a local nature had to be accomplished. The first step was to attain safety approval for conduct of the experiment. Similiar approvals will be required for all future tests on the range. For that reason a portion of the safety studies for the HeNe laser and follow-on CO₂ lasers are included in this report. This information may be found in Appendices A, B, and C.

Much of the initial work in setting up the range involved selection and testing of equipment. The individual pieces of equipment are described in Chapter III of this report. Experimental arrangement and operation of the equipment are the subjects of Chapter IV.

In Chapter II, atmospheric attenuation and the effects of turbulence are discussed. Attenuation limited the amount of laser radiation which

reached the target plane. Turbulence produced movement and breakup of the beam upon the target plane. Both effects could limit the amount of power which was detected at the target.

Types of attenuation which are discussed are molecular absorption, molecular scattering, aerosol absorption, and aerosol scattering. If a standard weather model was used, predictions of resulting attenuation from each of these effects could be taken from tables developed from a computer model called Hitran (Ref 9).

Hitran could not, however, be used to estimate the effect atmospheric turbulence would have upon experimental results. This had to be predicted from the observations made in previous studies. During first stage operation with the HeNe laser an attempt was made to minimize the effect of turbulence, so that attenuation could be studied independently. Later testing may include, or focus upon, these secondary effects.

Several assumptions were made during the theoretical development and during data interpretation. One was that the theoretical attenuation coefficients given by McClatchey and Selby (Ref 9, Tables 1, 2, and 3 of this report) for altitude block 0-1 km were applicable to the actual experimental setup. During the test the laser beam followed a path that varied from 354 to 266 meters above sea level. An interpolation between altitudes was possible with the theoretical models, but was not considered necessary in this report due to the small altitude differences involved.

Another assumption was made during visibility measurements. During each test run an estimate of visibility was made by observation of local landmarks from the transmitter site in the tower of Building 620. This method seemed to produce more reliable estimates than those obtained from the base weather service. An assumption was made during the

observations that visibility along the test path was the same as along the entire path out to the limits of vision. An observation of 5 km visibility would be meaningless if a localized occurrence, such as a rainshower, existed only over a portion of the area of view. For this reason, tests were conducted only during periods when atmospheric uniformity was observed.

A third assumption was that secondary scattering by molecular and aerosol constituents of the air had a negligible effect upon the amount of light which reached the target. Secondary scattering refers to secondary deflection of light, which has been deflected away from the target, back toward the target. The effect is quite complicated and is not included in Hitran attenuation models. According to W. Middleton, however, secondary scattering effects are minimal when the divergence of the beam and the field of view of the detector are as small as those found in the experimental setup used during these tests. In the experiment the field of view of the detector was approximately 5 milliradians and the beam divergence was .03 milliradians. For these figures the resulting error introduced by secondary scattering into transmission measurements should be less than 1.0% (Ref 10: 576).

During the tests the method used to experimentally investigate atmospheric attenuation was to measure total power transfer. The relationship between attenuation and power transfer over a distance, R , is given by the following equation:

$$T = \exp(-\gamma R) \quad (1)$$

where γ is the attenuation coefficient and T is transmittance, the fraction of power transferred (Ref 8, 9). To experimentally determine T , measurements of power transfer over a short range, where T was

assumed to be unity, were compared to those over a long range. In both cases the same optical equipment was used, and it was possible to capture the entire beam and focus it upon the detector. The short range measurement, therefore, was the standard for all transmission calculations.

The approach that was taken during the experiment was as follows: (1) laboratory testing of equipment, (2) field calibrations, (3) range alignment, (4) data collection, and (5) comparison of test results to theoretical predictions.

The first piece of equipment to be tested in the lab was the laser. It was necessary to determine if there were fluctuations in power output. If fluctuations existed, the beam leaving the laser would have to be monitored constantly during test runs. If not, laser power could be assumed to be constant.

The operational characteristics of all other equipment, which was to be used on the range setup, were also examined. It was desirable to discover any problem areas while the equipment was assembled in one place. The last operation which was completed prior to range installation was an initial determination of the power measurement to be associated with 100% transmission. This was easily achieved in the lab by positioning the transmitter and receiver within a few meters of each other.

During field calibration the short range measurement was reaccomplished. This was done to certify that the operating characteristics of the equipment in its new environment were known.

Range alignment was achieved by visual means. An observer at the receiver gave instructions to the laser operator for movement of the beam. The instructions were implemented by adjusting azimuth and tilt controls on

the mount which held the laser.

With the equipment operational, data was taken on as many occasions as time and weather permitted. Results were compared to the theoretical predictions of McClatchey and Selby (Ref 9).

II. Theory

Atmospheric attenuation of laser radiation and the effect that air turbulence has upon beam propagation are the topics of this chapter. A discussion is included of computer models which can be used to predict the amount of attenuation produced by different weather conditions.

Atmospheric Attenuation

Electromagnetic radiation in the form of laser radiation has both wave and particle characteristics. Consideration of light to be composed of photons, however, facilitates discussion of the interaction of a laser beam with constituents of the air along the path of propagation. Therefore, atmospheric attenuation will be considered to result from interaction of laser photons with gas molecules and aerosol particles. During these interactions the photons are absorbed or scattered. The resulting attenuation can be described by the following equation, which was mentioned in the introduction:

$$T = \exp(-\gamma R) \quad (1)$$

where T is monochromatic transmittance, γ is the total attenuation coefficient, and R the range length (Ref 7, 8, 9). The total attenuation coefficient, γ , includes separate coefficients, which are generally additive. This is demonstrated by the following equation:

$$\gamma = \delta + K \quad (2)$$

where δ is the scattering coefficient, and K the absorption coefficient. Also, each of δ and K is a sum of molecular and aerosol coefficients.

That is, γ and K are defined by the following equations:

$$\delta = \delta_m + \delta_a \quad (3)$$

$$K = K_m + K_a \quad (4)$$

where the subscripts, m and a, indicate molecular and aerosol respectively. Estimates of the size of each of these coefficients can be taken from tables contained in a report by McClatchey and Selby (Ref 9: 15-26). On following pages, Tables I, II, and III reproduce the attenuation predictions for three laser wavelengths: (1) HeNe (.6328 u), (2) Nd:YAG (1.06 u), and (3) CO₂ (10.59 u). Five model atmospheres and two aerosol models are included. The coefficients are given for one kilometer altitude blocks from sea level to 25 km, and for larger blocks above 25 km. The tables are referred to on numerous occasions in different sections of this report.

Molecular Scattering. Molecular scattering refers to reflection of laser photons from gas molecules. The molecular scattering coefficient depends only on the number density of molecules along the radiation path. The wavelength dependency of molecular scattering is very nearly $\delta_m \sim \lambda^{-4}$ (Ref 9: 11). As can be seen in Tables I-III, this means that while molecular scattering produces a small amount of attenuation for HeNe and Nd:YAG radiation, it produces almost no attenuation for the longer wavelength, CO₂ radiation.

Molecular Absorption. This type of absorption can occur when the incident photon, vibrating at the laser frequency, interacts with a gas molecule which has a similar transition, or resonant, frequency. The probability of absorption is determined by the type and number of gas molecules present, and by their energy states before interaction. Atmospheric temperature and pressure can be used to predict energy states. The important molecule types are (in order of importance) H₂O, CO₂, O₃, N₂O, CO, O₂, CH₄, and N₂. All of these, except H₂O and O₃, are assumed to be uniformly mixed by volume. Concentrations of H₂O and

Table I
Attenuation Coefficients for HeNe Laser

H ₀ (mm)	TROPICAL		MIDLATITUDE SUMMER		MIDLATITUDE WINTER		SUBARCTIC SUMMER		SUBARCTIC WINTER		AEROSOL CLEAR		AEROSOL HAZY	
	k_m (km ⁻¹)	σ_m (km ⁻¹)	k_m (km ⁻¹)	σ_m (km ⁻¹)	k_m (km ⁻¹)	σ_m (km ⁻¹)	k_m (km ⁻¹)	σ_m (km ⁻¹)	k_m (km ⁻¹)	σ_m (km ⁻¹)	k_m (km ⁻¹)	σ_m (km ⁻¹)	k_m (km ⁻¹)	σ_m (km ⁻¹)
0	<E-06	6.31E-03	<E-06	6.79E-03	<E-06	6.58E-03	<E-06	7.37E-03	3.14E-03	1.36E-01	1.53E-02	6.63E-01	6.63E-02	
0-1		6.03E-03		6.62E-03		6.28E-03		6.88E-03	2.09E-03	9.03E-02	9.26E-03	4.01E-01	9.26E-03	
1-2		5.49E-03		5.91E-03		5.66E-03		6.04E-03	3.93E-03	3.39E-02	3.39E-03	1.47E-01	3.39E-03	
2-3		4.97E-03		5.26E-03		5.10E-03		5.36E-03	3.87E-04	1.67E-02	1.24E-03	5.36E-02	1.24E-03	
3-4		4.49E-03		4.70E-03		4.58E-03		4.75E-03	1.82E-04	7.89E-03	4.52E-04	1.96E-02	4.52E-04	
4-5		4.07E-03		4.21E-03		4.11E-03		4.24E-03	1.15E-04	4.98E-03	1.65E-04	7.14E-03	1.65E-04	
5-6		3.68E-03		3.76E-03		3.69E-03		3.79E-03	8.39E-05	3.63E-03	8.39E-05	3.63E-03	8.39E-05	
6-7		3.31E-03		3.35E-03		3.32E-03		3.37E-03	6.78E-05	2.94E-03	6.78E-05	2.94E-03	6.78E-05	
7-8		2.98E-03		2.98E-03		2.97E-03		2.99E-03	6.65E-05	2.88E-03	6.65E-05	2.88E-03	6.65E-05	
8-9		2.67E-03		2.66E-03		2.66E-03		2.67E-03	6.61E-05	2.86E-03	6.61E-05	2.86E-03	6.61E-05	
9-10		2.39E-03		2.37E-03		2.36E-03		2.36E-03	6.39E-05	2.77E-03	6.39E-05	2.77E-03	6.39E-05	
10-11		2.13E-03		2.11E-03		2.03E-03		1.93E-03	6.11E-05	2.64E-03	6.11E-05	2.64E-03	6.11E-05	
11-12		1.89E-03		1.74E-03		1.78E-03		1.65E-03	6.06E-05	2.62E-03	6.06E-05	2.62E-03	6.06E-05	
12-13		1.66E-03		1.48E-03		1.49E-03		1.41E-03	5.87E-05	2.58E-03	5.87E-05	2.58E-03	5.87E-05	
13-14		1.48E-03		1.28E-03		1.28E-03		1.21E-03	5.67E-05	2.45E-03	5.67E-05	2.45E-03	5.67E-05	
14-15		1.30E-03		1.23E-03		1.10E-03		1.03E-03	5.44E-05	2.35E-03	5.44E-05	2.35E-03	5.44E-05	
15-16		1.13E-03		1.04E-03		9.41E-04		8.82E-04	5.14E-05	2.23E-03	5.14E-05	2.23E-03	5.14E-05	
16-17		9.78E-04		8.92E-04		8.07E-04		7.56E-04	4.89E-05	2.16E-03	4.89E-05	2.16E-03	4.89E-05	
17-18		8.20E-04		7.63E-04		6.91E-04		6.47E-04	4.68E-05	2.11E-03	4.68E-05	2.11E-03	4.68E-05	
18-19		6.77E-04		6.51E-04		5.91E-04		5.54E-04	4.40E-05	1.91E-03	4.40E-05	1.91E-03	4.40E-05	
19-20		5.62E-04		5.65E-04		5.06E-04		4.75E-04	3.46E-05	1.50E-03	3.46E-05	1.50E-03	3.46E-05	
20-21		4.68E-04		4.73E-04		4.32E-04		4.06E-04	2.52E-05	1.09E-03	2.52E-05	1.09E-03	2.52E-05	
21-22		3.91E-04		4.03E-04		3.69E-04		3.47E-04	1.87E-05	8.07E-04	1.87E-05	8.07E-04	1.87E-05	
22-23		3.29E-04		3.44E-04		3.15E-04		2.97E-04	1.42E-05	6.13E-04	1.42E-05	6.13E-04	1.42E-05	
23-24		2.79E-04		2.93E-04		2.68E-04		2.54E-04	1.10E-05	4.77E-04	1.10E-05	4.77E-04	1.10E-05	
24-25		2.37E-04		2.51E-04		2.30E-04		2.17E-04	9.00E-06	3.90E-04	9.00E-06	3.90E-04	9.00E-06	
25-30		1.58E-04		1.68E-04		1.53E-04		1.44E-04	4.53E-06	1.96E-04	4.53E-06	1.96E-04	4.53E-06	
30-35		7.22E-05		7.76E-05		6.80E-05		6.39E-05	1.28E-06	5.52E-05	1.28E-06	5.52E-05	1.28E-06	
35-40		3.43E-05		3.69E-05		3.10E-05		2.87E-05	<E-06	1.45E-05	<E-06	1.45E-05	<E-06	
40-45		1.68E-05		1.82E-05		1.44E-05		1.22E-05	3.83E-06	3.83E-06	3.83E-06	3.83E-06	3.83E-06	
45-50		3.57E-06		9.31E-06		7.06E-06		6.23E-06	1.01E-06	1.01E-06	1.01E-06	1.01E-06	1.01E-06	
50-70		3.20E-06		3.51E-06		2.59E-06		2.32E-06	<E-06	<E-06	<E-06	<E-06	<E-06	
70-100		<E-06		<E-06		<E-06		<E-06	<E-06	<E-06	<E-06	<E-06	<E-06	

(From Ref 9: 18)

Table II
Attenuation Coefficients for Nd:YAG Laser

$\lambda = 1.06 \mu\text{m}$

Ht (km)	TROPICAL		MIDLATITUDE SUMMER		MIDLATITUDE WINTER		SUBARCTIC SUMMER		SUBARCTIC WINTER		AEROSOL CLEAR		AEROSOL HAZY	
	k_m (km^{-1})	σ_m (km^{-1})	k_m (km^{-1})	σ_m (km^{-1})	k_m (km^{-1})	σ_m (km^{-1})	k_m (km^{-1})	σ_m (km^{-1})	k_m (km^{-1})	σ_m (km^{-1})	k_m (km^{-1})	σ_m (km^{-1})	k_m (km^{-1})	σ_m (km^{-1})
0	<E-06	8.04E-04	<E-06	8.20E-04	<E-06	8.91E-04	<E-06	8.38E-04	9.39E-04	1.99E-02	6.79E-02	9.63E-02	9.63E-02	3.31E-01
0-1		7.68E-04		7.81E-04		8.43E-04		7.98E-04	9.77E-04	1.31E-02	4.50E-02	5.82E-02	5.82E-02	2.00E-01
1-2		6.99E-04		7.06E-04		7.52E-04		7.21E-04	7.70E-04	5.71E-03	1.96E-02	2.13E-02	2.13E-02	7.31E-02
2-3		6.33E-04		6.38E-04		6.70E-04		6.50E-04	6.82E-04	2.43E-03	8.36E-03	7.78E-03	7.78E-03	2.67E-02
3-4		5.72E-04		5.77E-04		5.99E-04		5.84E-04	6.06E-04	1.15E-03	3.94E-03	2.84E-03	2.84E-03	9.76E-03
4-5		5.19E-04		5.21E-04		5.37E-04		5.24E-04	5.40E-04	7.22E-04	2.49E-03	1.04E-03	1.04E-03	3.56E-03
5-6		4.69E-04		4.69E-04		4.80E-04		4.71E-04	4.82E-04	5.27E-04	1.81E-03	5.27E-04	5.27E-04	1.81E-03
6-7		4.22E-04		4.21E-04		4.27E-04		4.23E-04	4.29E-04	4.17E-04	1.47E-03	4.27E-04	4.27E-04	1.47E-03
7-8		3.80E-04		3.78E-04		3.80E-04		3.79E-04	3.81E-04	4.18E-04	1.44E-03	4.18E-04	4.18E-04	1.44E-03
8-9		3.41E-04		3.38E-04		3.36E-04		3.38E-04	3.34E-04	4.15E-04	1.43E-03	4.15E-04	4.15E-04	1.43E-03
9-10		3.04E-04		3.02E-04		2.97E-04		3.01E-04	2.88E-04	4.01E-04	1.38E-03	4.01E-04	4.01E-04	1.38E-03
10-11		2.72E-04		2.69E-04		2.59E-04		2.64E-04	2.46E-04	3.84E-04	1.32E-03	3.84E-04	3.84E-04	1.32E-03
11-12		2.41E-04		2.39E-04		2.22E-04		2.26E-04	2.10E-04	3.81E-04	1.31E-03	3.81E-04	3.81E-04	1.31E-03
12-13		2.13E-04		2.11E-04		1.90E-04		1.95E-04	1.80E-04	3.75E-04	1.29E-03	3.75E-04	3.75E-04	1.29E-03
13-14		1.88E-04		1.83E-04		1.63E-04		1.67E-04	1.54E-04	3.56E-04	1.23E-03	3.56E-04	3.56E-04	1.22E-03
14-15		1.66E-04		1.56E-04		1.40E-04		1.44E-04	1.31E-05	3.42E-04	1.18E-03	3.42E-04	3.42E-04	1.18E-03
15-16		1.44E-04		1.33E-04		1.20E-04		1.23E-04	1.12E-05	3.23E-04	1.11E-03	3.23E-04	3.23E-04	1.11E-03
16-17		1.24E-04		1.14E-04		1.03E-04		1.06E-04	9.63E-05	3.13E-04	1.09E-03	3.13E-04	3.13E-04	1.08E-03
17-18		1.05E-04		9.72E-05		8.80E-05		9.14E-05	8.25E-05	3.06E-04	1.05E-03	3.06E-04	3.06E-04	1.05E-03
18-19		8.63E-05		8.29E-05		7.53E-05		7.66E-05	7.06E-05	2.77E-04	9.51E-04	2.77E-04	2.77E-04	9.51E-04
19-20		7.16E-05		7.07E-05		6.45E-05		6.75E-05	6.05E-05	2.18E-04	7.48E-04	2.18E-04	2.18E-04	7.48E-04
20-21		5.96E-05		6.02E-05		5.51E-05		5.80E-05	5.17E-05	1.59E-04	5.45E-04	1.59E-04	1.59E-04	5.45E-04
21-22		4.98E-05		5.14E-05		4.70E-05		4.99E-05	4.42E-05	1.17E-04	4.03E-04	1.17E-04	1.17E-04	4.03E-04
22-23		4.19E-05		4.36E-05		4.01E-05		4.29E-05	3.78E-05	8.89E-04	3.06E-04	8.89E-04	8.89E-04	3.06E-04
23-24		3.55E-05		3.74E-05		3.43E-05		3.69E-05	3.23E-05	6.93E-05	2.38E-04	6.93E-05	6.93E-05	2.38E-04
24-25		3.02E-05		3.19E-05		2.93E-05		3.15E-05	2.76E-05	5.66E-05	1.94E-04	5.66E-05	5.66E-05	1.94E-04
25-30		2.01E-05		2.15E-05		1.94E-05		2.13E-05	1.84E-05	2.85E-05	9.79E-05	2.85E-05	2.85E-05	9.79E-05
30-35		9.20E-06		9.89E-06		8.78E-06		9.98E-06	8.14E-06	8.02E-06	2.76E-05	8.02E-06	8.02E-06	2.76E-05
35-40		4.37E-06		4.71E-06		3.96E-06		4.73E-06	3.66E-06	2.11E-06	7.26E-06	2.11E-06	7.26E-06	2.11E-06
40-45		2.15E-06		2.31E-06		1.83E-06		2.33E-06	1.68E-06	9.19E-06	2.11E-06	9.19E-06	9.19E-06	2.11E-06
45-50		1.08E-06		1.19E-06		<E-06		1.21E-06	<E-06	<E-06	<E-06	<E-06	<E-06	<E-06
50-70		<E-06		<E-06		<E-06		<E-06	<E-06	<E-06	<E-06	<E-06	<E-06	<E-06
70-100														

(From Ref 9: 21)

Table III
Attenuation Coefficients for CO₂ Laser

$\lambda = 10.591 \mu\text{m}$

Ht(ftm)	TROPICAL		MIDLATITUDE SUMMER		MIDLATITUDE WINTER		SUBARCTIC SUMMER		SUBARCTIC WINTER		CLEAR		AEROSOL		HAZY	
	k_m (ftm ⁻¹)	σ_m (ftm ⁻¹)	k_m (ftm ⁻¹)	σ_m (ftm ⁻¹)	k_m (ftm ⁻¹)	σ_m (ftm ⁻¹)	k_m (ftm ⁻¹)	σ_m (ftm ⁻¹)	k_m (ftm ⁻¹)	σ_m (ftm ⁻¹)	k_m (ftm ⁻¹)	σ_m (ftm ⁻¹)	k_m (ftm ⁻¹)	σ_m (ftm ⁻¹)	k_m (ftm ⁻¹)	σ_m (ftm ⁻¹)
0	5.38E-01	<1.0E-06	3.28E-01	<1.0E-06	5.89E-02	<1.0E-06	1.73E-01	<1.0E-06	3.01E-02	<1.0E-06	5.48E-03	4.65E-03	2.87E-02	2.27E-02	2.87E-02	2.27E-02
0-1	4.10E-01		2.50E-01		5.21E-02		1.36E-01		2.84E-02		3.64E-03	3.09E-03	1.61E-02	1.37E-02	1.61E-02	1.37E-02
1-2	2.44E-01		1.37E-01		4.05E-02		8.39E-02		2.67E-02		1.58E-03	1.34E-03	5.90E-03	5.01E-03	5.90E-03	5.01E-03
2-3	1.21E-01		7.89E-02		3.27E-02		5.66E-02		2.30E-02		6.75E-04	5.73E-04	2.16E-03	1.83E-03	2.16E-03	1.83E-03
3-4	6.29E-02		5.02E-02		2.60E-02		4.07E-02		1.95E-02		3.18E-04	2.70E-04	7.88E-04	6.88E-04	7.88E-04	6.88E-04
4-5	4.14E-02		3.58E-02		2.07E-02		3.03E-02		1.55E-02		2.01E-04	1.70E-04	2.88E-04	2.44E-04	2.88E-04	2.44E-04
5-6	3.23E-02		2.86E-02		1.66E-02		2.38E-02		1.22E-02		1.46E-04	1.24E-04	1.46E-04	1.24E-04	1.46E-04	1.24E-04
6-7	2.54E-02		2.38E-02		1.36E-02		1.82E-02		9.55E-03		1.18E-04	1.00E-04	1.18E-04	1.00E-04	1.18E-04	1.00E-04
7-8	2.01E-02		1.90E-02		1.09E-02		1.43E-02		7.39E-03		1.16E-04	9.83E-05	1.16E-04	9.83E-05	1.16E-04	9.83E-05
8-9	1.65E-02		1.49E-02		8.84E-03		1.12E-02		6.05E-03		1.15E-04	9.77E-05	1.15E-04	9.77E-05	1.15E-04	9.77E-05
9-10	1.30E-02		1.22E-02		6.82E-03		8.64E-03		5.64E-03		1.11E-04	9.45E-05	1.11E-04	9.45E-05	1.11E-04	9.45E-05
10-11	1.03E-02		9.87E-03		6.20E-03		7.53E-03		5.64E-03		1.06E-04	9.04E-05	1.06E-04	9.04E-05	1.06E-04	9.04E-05
11-12	8.11E-03		7.82E-03		5.99E-03		7.75E-03		5.63E-03		1.06E-04	8.96E-05	1.06E-04	8.96E-05	1.06E-04	8.96E-05
12-13	6.54E-03		6.03E-03		5.91E-03		7.45E-03		5.52E-03		1.04E-04	8.83E-05	1.04E-04	8.83E-05	1.04E-04	8.83E-05
13-14	4.67E-03		5.28E-03		5.80E-03		7.76E-03		5.76E-03		9.89E-05	8.39E-05	9.89E-05	8.39E-05	9.89E-05	8.39E-05
14-15	3.71E-03		5.50E-03		5.69E-03		7.72E-03		5.62E-03		9.49E-05	8.05E-05	9.49E-05	8.05E-05	9.49E-05	8.05E-05
15-16	2.75E-03		5.37E-03		5.53E-03		7.36E-03		5.55E-03		8.97E-05	7.61E-05	8.97E-05	7.61E-05	8.97E-05	7.61E-05
16-17	2.10E-03		5.29E-03		5.42E-03		7.68E-03		5.41E-03		8.69E-05	7.38E-05	8.69E-05	7.38E-05	8.69E-05	7.38E-05
17-18	2.26E-03		5.36E-03		5.41E-03		7.60E-03		5.27E-03		8.50E-05	7.21E-05	8.50E-05	7.21E-05	8.50E-05	7.21E-05
18-19	2.76E-03		5.42E-03		5.22E-03		7.58E-03		5.20E-03		7.68E-05	6.51E-05	7.68E-05	6.51E-05	7.68E-05	6.51E-05
19-20	3.30E-03		5.65E-03		5.07E-03		7.69E-03		4.99E-03		6.04E-05	5.12E-05	6.04E-05	5.12E-05	6.04E-05	5.12E-05
20-21	3.98E-03		5.81E-03		5.19E-03		7.50E-03		4.93E-03		4.40E-05	3.74E-05	4.40E-05	3.74E-05	4.40E-05	3.74E-05
21-22	4.74E-03		6.15E-03		5.19E-03		7.64E-03		4.77E-03		3.25E-05	2.76E-05	3.25E-05	2.76E-05	3.25E-05	2.76E-05
22-23	5.29E-03		6.40E-03		5.18E-03		7.64E-03		4.57E-03		2.47E-05	2.09E-05	2.47E-05	2.09E-05	2.47E-05	2.09E-05
23-24	5.73E-03		7.06E-03		5.15E-03		7.58E-03		4.65E-03		1.92E-05	1.63E-05	1.92E-05	1.63E-05	1.92E-05	1.63E-05
24-25	6.29E-03		7.05E-03		5.32E-03		8.08E-03		4.34E-03		1.57E-05	1.33E-05	1.57E-05	1.33E-05	1.57E-05	1.33E-05
25-30	7.65E-03		8.43E-03		5.14E-03		9.23E-03		4.61E-03		7.90E-06	6.71E-06	7.90E-06	6.71E-06	7.90E-06	6.71E-06
30-35	7.57E-03		8.38E-03		4.36E-03		1.28E-02		3.66E-03		2.23E-06	1.89E-06	2.23E-06	1.89E-06	2.23E-06	1.89E-06
35-40	7.01E-03		8.08E-03		4.29E-03		8.88E-03		3.18E-03		<1.0E-06	<1.0E-06	<1.0E-06	<1.0E-06	<1.0E-06	<1.0E-06
40-45	5.65E-03		6.77E-03		3.85E-03		7.57E-03		2.61E-03							
45-50	3.85E-03		4.79E-03		2.81E-03		5.22E-03		1.97E-03							
50-70	5.75E-03		6.87E-04		1.75E-04		7.00E-04		4.85E-04							
70-100	9.40E-06		1.13E-05		1.00E-05		1.13E-05		1.14E-05							

(From Ref 9: 24)

O_3 are functions of altitude and temperature (Ref 9: 11). Tables exist from which the predicted concentrations of the uniformly mixed gases can be taken, as well as the predicted concentrations of H_2O and O_3 under six model atmospheric conditions (Ref 9: 3-8).

Each of the molecules has characteristic transition frequencies at which energy can be absorbed. Normally the frequency widths are narrow, thus producing sharp absorption lines. The H_2O molecule, however, provides an absorption continuum in the 8-13 μm and in the 16-30 μm regions (Ref 8: 2). The combination of all sharp absorption lines and the H_2O continua is a series of absorption peaks and valleys across the wavelength spectrum. The presence or absence of a continuum determines the depth of the regions, called transmission windows, between absorption peaks. The amount of attenuation caused by molecular absorption is therefore strongly dependent upon the operating frequency of the laser. As can be seen in Tables I-III, molecular absorption is responsible for the greatest amount of CO_2 attenuation, but it produces only minor attenuation for the HeNe and Nd:YAG lasers.

Aerosol Attenuation. Aerosols are small solid and liquid particles which are suspended in the air. Under severe conditions they can produce the dominate type of attenuation (Ref 14). Two aerosol models, to describe "clear" and "hazy" days, are included in the tabulated results of McClatchey and Selby. In the 0-1 km altitude block a "clear" day refers to 23 km visibility and a "hazy" day to 5 km visibility (Ref 9).

The aerosol scattering and absorption coefficients are functions of the number of particles present, their size distributions, and their complex indices of refraction. The rather involved theory of scattering was first worked out by Mie for spherical particles (Ref 11), and a

comprehensive study of Mie scattering was done by Van de Hulst (Ref 16). Absorption coefficients can be similarly derived, and the derivations may be found in several articles (Ref 6: 181)(Ref 9: 11-13). For the purposes of this report, the "clear" and "hazy" day models of McClatchey and Selby will provide sufficient data to make predictions of the expected amount of aerosol attenuation.

Reference to Table I shows that for the HeNe laser, aerosol scattering produces the dominate type of attenuation in the 0-1 km altitude block. In fact, the aerosol scattering coefficient on "hazy" days is 100 times as large as all other combined coefficients and is 10 times as large on clear days. Because of this dominance, the scattering coefficients for a "clear" and a "hazy" day in the 0-1 km block can be used to predict transmission values for different visibility conditions encountered in the experimental setup.

For laser radiation in the visible portion of the spectrum, such as HeNe radiation, the relationship between transmission and visibility can be approximated by the following equation (Ref 2: 2.55):

$$v = 3.9/(\text{scat. coeff.}) \quad (5)$$

As can be seen from the equation, there is a linear relationship between visibility and $(\text{scat. coeff.})^{-1}$. Using this relationship, a graph of visibility versus $(\text{scat. coeff.})^{-1}$ can be made. A straight line is drawn between the $(\text{scat. coeff.})^{-1}$ values for 5 and 23 km visibilities, as given by McClatchey and Selby. From the graph it is then possible to predict coefficients relating to a range of visibility conditions. These coefficients can then be converted to expected transmission values. The result is depicted in Figure 2, where expected transmission rates are plotted against visibility. Later in Chapter V

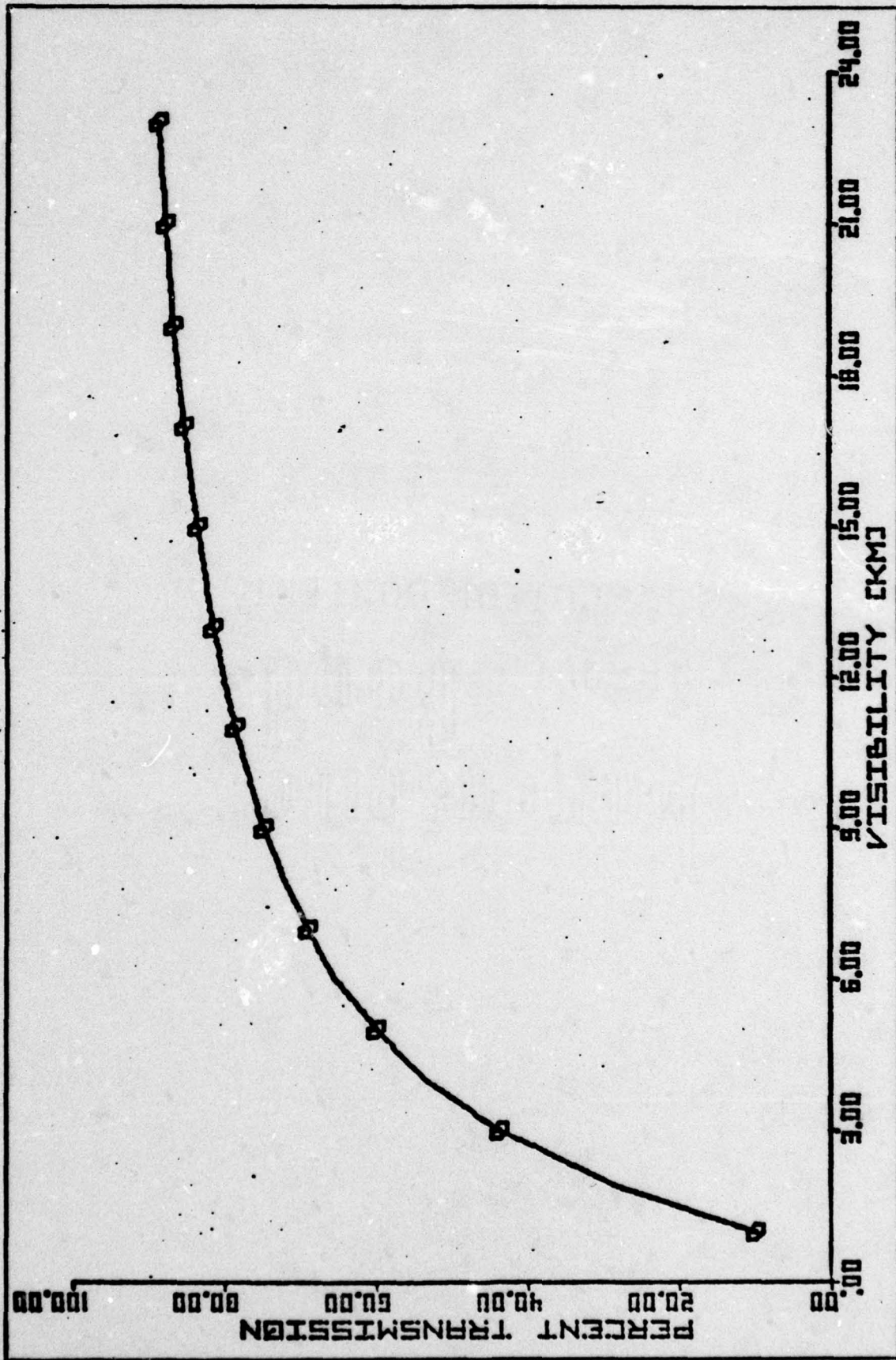


Fig. 2. Theoretical Transmission Versus Visibility for HeNe Laser

this figure will be used for the comparison of theoretical and experimental results.

Effects of Atmospheric Turbulence

Turbulent air is an inhomogeneous mixture of gases and suspended particles, in which localized composition varies with position and time. Different regions display different indices of refraction to passing light. The effect upon a laser beam is random alteration of the beam's amplitude, phase, and direction (Ref 4: 135).

Turbulence and its consequences normally are most pronounced in the low altitude region, where the air-ground interface produces numerous eddies of varying composition. This is, of course, the region in which the laser tests were to be conducted.

As was mentioned in Chapter I, during experimentation using the HeNe laser, an attempt was made to minimize the effect atmospheric turbulence had upon test results. Study of turbulence effects was confined to observation of the amount and type present, and to the limits thus imposed upon power transfer measurements. It was important, however, to understand the mechanics and magnitude of turbulence effects which were likely to be encountered. These included spot dancing, beam spreading, image dancing, and scintillations.

Spot Dancing. When the laser beam passes through large pockets of air in which the refractive index is different than the norm, the entire beam can be deviated from its original direction. The result is movement of the laser spot upon the target plane, called spot dancing. If the spot moves off the receiving optics, power deviations are recorded which are not the result of atmospheric attenuation.

The relationship between spot dancing and turbulence was examined

in experiments conducted by T. Gilmartin and J. Holtz (Ref 5). One of their findings was that on a normal, clear day the amount of beam wander (spot dancing) increased during the warm, turbulent part of the day and was at a minimum shortly before sunset and shortly after sunrise. The amount of observed diurnal variation is depicted in Figure 4. The tests were completed using a CO₂ laser on a 5.4 km range. On the graph, the spot radii, R_e and R_e', were radii of blurred spots on photographic film. The blurring was caused by spot dancing. Although the graph resulted from experiments conducted with a CO₂ laser, other lasers should produce similar diurnal variations.

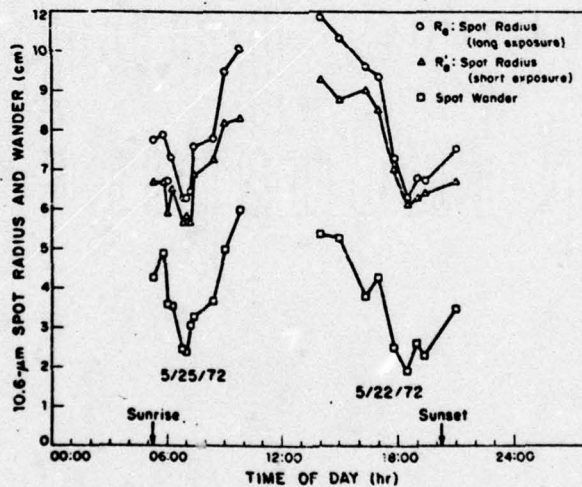


Fig. 3. Diurnal Variation of CO₂ Laser Spot Characteristics (From Ref 5: 1908)

T. Chiba furnishes an equation which may be used to estimate the amount of spot dancing likely to be encountered during different

turbulence conditions (Ref 3: 2457). According to his report, the standard deviation of the linear displacement, β_x , of the laser spot is given by the following equation:

$$\beta_x = .956 C_n z^{17/12} \lambda^{-1/12} \quad (6)$$

where λ is the laser wavelength, z is the length of the range, and C_n is the structure constant of the atmosphere. C_n is a function of atmospheric pressure and temperature, is dimensionless, and varies in magnitude from 5×10^{-7} for strong turbulence to 8×10^{-9} for weak turbulence (Ref 3: 2458). Using Equation 5, predicted β_x for HeNe radiation over a 1.23 km range during strong turbulence is 3.7 cm. Therefore, with sufficiently large receiver optics, it should be possible to eliminate the effects of spot dancing.

Beam Spreading. Another consequence of turbulence is small-angle scattering, which spreads the beam energy over a larger region. This occurs because the localized inhomogeneities produce changes in the divergence angle of the laser beam (Ref 4: 135).

A laser beam has a divergence angle, θ , which is characteristic of its propagation through free space. Using this divergence angle it is possible to estimate the spot size at the target plane by the following equation:

$$d = R \theta \quad (7)$$

where d is the beam diameter in the target plane, R is the range length, and θ is the full-cone divergence angle (Ref 18:171). For example, the test HeNe laser had a divergence angle of approximately 3×10^{-5} radians. Over a 1.23 km range the 3 cm beam was expected to increase in diameter to approximately 7 cm.

In the real atmosphere the divergence angle is dependent upon the

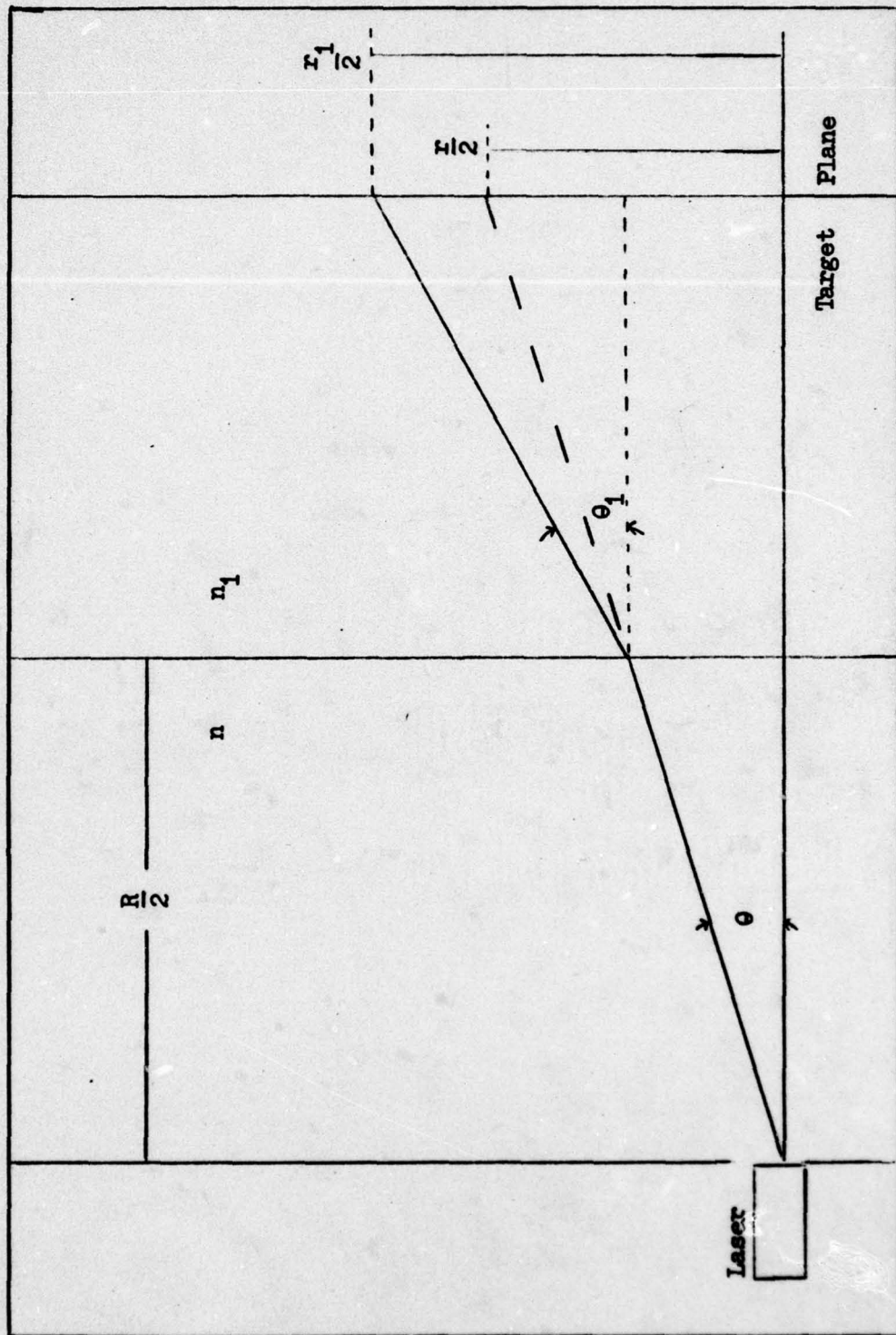


Fig. 4. Effect of Index of Refraction Change

refractive index of the air. Transmission through large pockets of air with nonstandard indices of refraction will produce changes in θ and corresponding changes in beam diameter. As an example, assume that halfway to the target the refractive index of the air changes at a plane surface boundary from 1.00 to 0.95. The following matrix can be used to approximate beam diameter at the target plane (Ref 13: 297):

$$\begin{bmatrix} r_1 \\ \theta_1 \end{bmatrix} = \begin{bmatrix} 1 & R/2 \\ 0 & 1 \end{bmatrix} \begin{bmatrix} 1 & 0 \\ 0 & n/n_1 \end{bmatrix} \begin{bmatrix} 1 & R/2 \\ 0 & 1 \end{bmatrix} \begin{bmatrix} r \\ \theta \end{bmatrix} \quad (8)$$

where $R = 1.23$ km

$$n/n_1 = 1/0.95 = 1.05$$

$$r = 3 \text{ cm}$$

$$\theta = 3 \times 10^{-5} \text{ radians}$$

Then $r_1 = 6.78$ cm

$$\theta_1 = 3.15 \times 10^{-5} \text{ radians}$$

Using this same matrix and assuming homogeneity, the target spot size is 6.69 cm. The two-index system produced a change of 1.3% in spot diameter. This example is illustrated in Figure 5.

The alteration in spot size would be larger for systems operating over longer ranges, and for those having larger free-space divergence angles. Also, during actual operation spot size is expected to fluctuate as turbulence produces eddies of varying composition along the path of propagation. For the HeNe laser which will be tested, fluctuations should normally be only a small fraction of the average beam diameter. Therefore, since the receiver was several times larger than the beam diameter, beam spreading was expected to have only minimal effect upon power measurements.

Image Dancing. Receiving optics focused the laser beam unto a detector positioned in the focal plane. Variations in the arrival angle of the beam could cause movement of the focused spot. J. Davis provides the following equation for estimating the maximum image movement which could be expected (Ref 4: 151):

$$x = 3 f \alpha \quad (9)$$

where x = maximum image displacement

f = focal length of receiving optic

α = maximum tilt angle of arriving beam

The tilt angle α is a function of range length and beam diameter. For a one kilometer range and a 5 cm beam diameter, α is given by Davis to be 3.56 microradians. Therefore, maximum beam displacement should be only .02 millimeters, if the focal length of the receiving optic is 2 meters. Davis concluded that displacement of the image from the focal point should almost always be negligible.

The effect of image dancing may have been larger during actual testing than the above calculations suggest. One factor not yet included in the calculations is the quality of the surface of the receiving optic. Movement of the beam upon a nonperfect surface may produce larger than expected displacement of the focused spot. Another possible factor is the size of the focused spot compared to that of the detector surface. If the detector area is only slightly larger than the spot size, small displacements may produce variations in detected output, which are unrelated to atmospheric attenuation. The same thing can occur if the detector surface is not uniformly sensitive.

Scintillation. Local inhomogenities along the path of propagation, which are smaller than the beam diameter, produce random amplitude

fluctuations within the wave front of the beam. The result is constructive and destructive interference, with corresponding bright and dark areas being projected onto the target plane. The effect is called scintillation. J. Davis gives the following equation from which the amount of amplitude fluctuation, X_a , can be estimated (Ref 4: 140):

$$X_a^2 = 0.31 C_n^2 k^{7/6} R^{11/6} \quad (10)$$

where C_n = atmospheric structure constant

$$k = 2\pi / (\text{wavelength})$$

$$R = \text{range length}$$

Fluctuations in amplitude are related to fluctuations in the logarithmic level of intensity, X_i , by the following equation (Ref 4: 140):

$$X_i^2 = 4 X_a^2 \quad (11)$$

The amount of fluctuation in received power, however, is strongly dependent upon the size of the detector aperture. A detector with an aperture which is smaller than the beam diameter will see bright and dark areas within the beam. The result will be large fluctuations in power output. On the other hand, power fluctuations can be made vanishingly small by increasing the receiver diameter until the entire beam is captured (Ref 4: 152).

According to Equation 9, amplitude fluctuations are directly proportional to range length and to the amount of turbulence, of which C_n is a measure, and are inversely proportional to wavelength. Therefore, CO_2 radiation should produce less scintillation than does the shorter wavelength HeNe radiation. The dependencies upon wavelength and upon range length are depicted in Figures 6 and 7. The included photographs depict instantaneous intensity distributions for focused HeNe and CO_2 laser beams over range lengths of 1.3 km, 5.05 km, and 8.6 km. Each

of the pictures was taken during conditions of medium turbulence, and with an output beam diameter of 30 cm (Ref 12: 7-12).

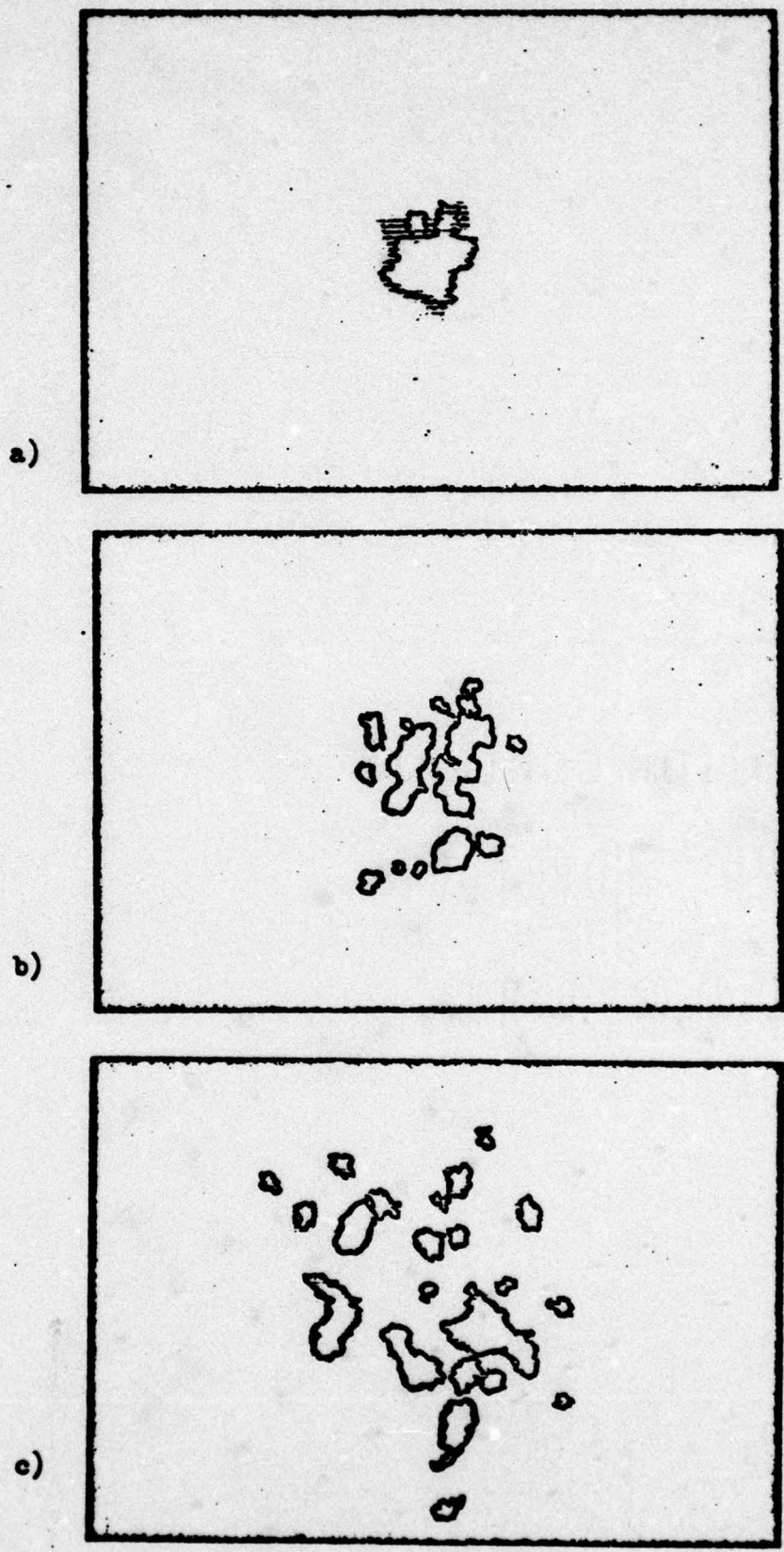


Fig. 5. Intensity Distribution of Focused Laser Beam at 0.63 μm
Measuring Conditions: Median Turbulence; Diameter = 30cm
a) $L = 1.3$ km; b) $L = 5.05$ km; c) $L = 8.6$ km (Ref 12)

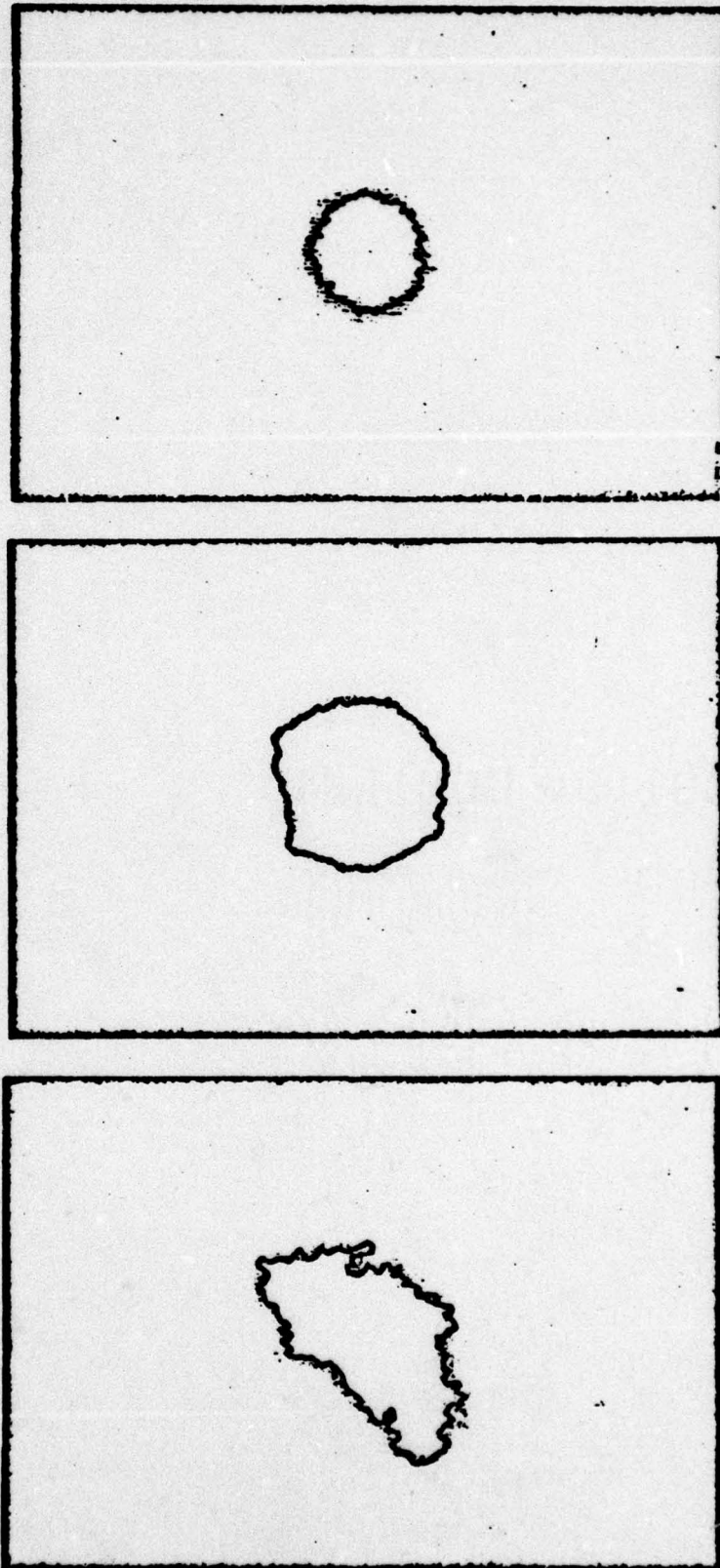


Fig. 6. Intensity Distribution of Focused Laser Beam at 10.6 μm
Measuring Conditions: Median Turbulence; Diameter = 30 cm
a) $L = 1.3$ km; b) $L = 5.05$ km; c) $L = 8.6$ km. (Ref 12)

III. Equipment

This chapter includes a description of equipment used to measure atmospheric attenuation of HeNe laser radiation. The equipment is categorized into those items used for transmission and those used for reception of the laser light. In addition, a description is included of extra equipment which was required during calibration.

Transmitting Equipment

The radiation source for this phase of testing was a low-powered HeNe laser. Attached to the laser was a collimating telescope. The laser and telescope were mounted on a heavy metal platform, which had fine-adjustment controls that could be used for precision alignment. After the telescope, the laser light passed through a safety pipe before leaving the transmission site. The setup is illustrated in Figure 8 and Figure 9 on the next page.

HeNe Laser. A Spectra-Physics Model 132 HeNe laser, which produced a maximum of 2.3 milliwatts, was the radiation source. The laser was operated with the polarizing magnets removed. Visible red light (632.8 nm) of transverse mode TEM_{00} was emitted. The beam leaving the exit pupil had a diameter of approximately 0.8 millimeters and a full-cone divergence angle of approximately 1.0 milliradians at the $1/e^2$ intensity points.

The Model 132 has a self-contained high voltage power supply, which operates on standard 110 volt, 60 cycle line current. The laser tube and high voltage circuits are contained within a metal housing, which measures 40 X 14 X 10 cm. Protection from shocks is provided by an interlock on the bottom coverplate of the housing. The interlock disables the high

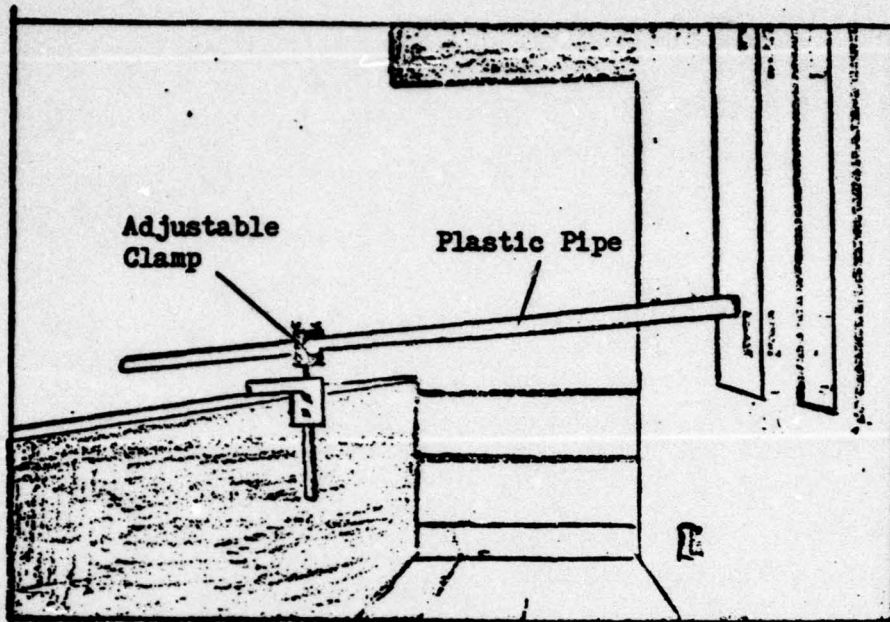


Fig. 7. Safety Pipe Mounted on Rail of Bldg. 620 Tower Balcony.

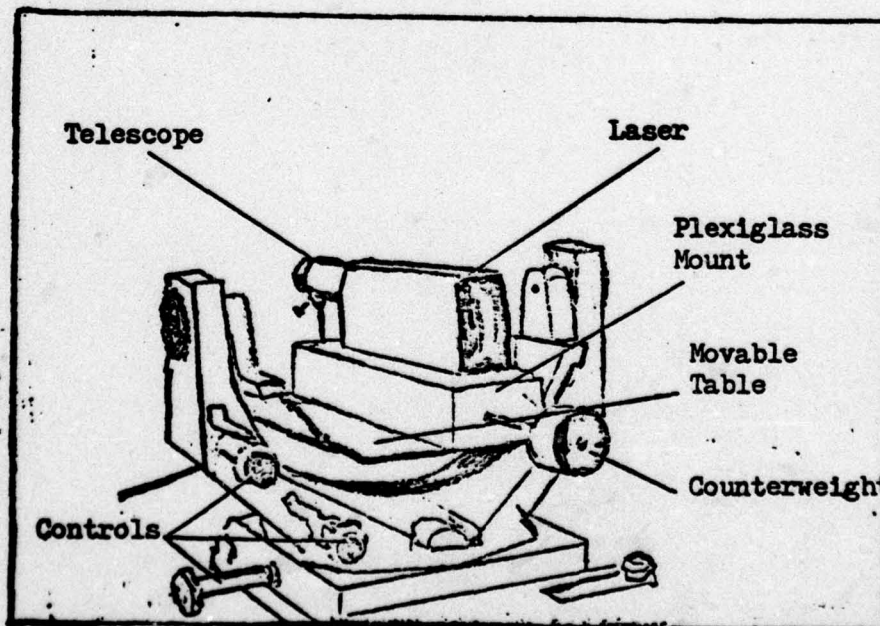


Fig. 8. Transmitter-Laser and Support

voltage power supply whenever the coverplate is removed. A circular steel mount is provided at the exit aperture of the laser, to which a Spectra-Physics Model 332/336 collimating telescope can be attached.

Laboratory testing demonstrated that when the laser was initially turned on, output fluctuated by approximately 2%. A warmup period of one hour reduced this fluctuation to a negligible magnitude.

Beam Expanding Telescope. The output of a HeNe laser closely approximates a Gaussian wavefront, and the far-field pattern for such a wavefront should also be Gaussian. The applicable beam divergence is given by the following equation:

$$\theta = (2 \lambda)/(d/2) \quad (12)$$

where θ is the full-cone divergence angle, λ is the laser wavelength, and d is the initial beam diameter at the $1/e^2$ intensity points (Ref 15:3.1).

During the experiment, the laser beam was to be projected over a long distance, and capture of the entire beam would facilitate measurement of total power transfer. Therefore, it was desirable to reduce the divergence given by Equation 11. This was accomplished by using a beam expanding telescope to enlarge the beam diameter prior to transmission. Thus, for a wavelength of 632.8 nm the expected divergence was decreased from 1 milliradian for the laser without a telescope, to .03 milliradians with a 3 cm diameter beam from the telescope. Using Equation 6 to calculate expected target spot size shows that a reduction from 1.23 meters to approximately 7 cm can be expected due to this decreased divergence.

The telescope consisted of a Spectra-Physics Model 336 collimator attached to a Model 332 beam expander. The beam expander was mounted directly on the laser exit aperture. Adjustment of the mount permitted

alignment of the beam with the telescope transmission axis. The 336/332 combination is illustrated in Figure 10, where all dimensions are given in centimeters.

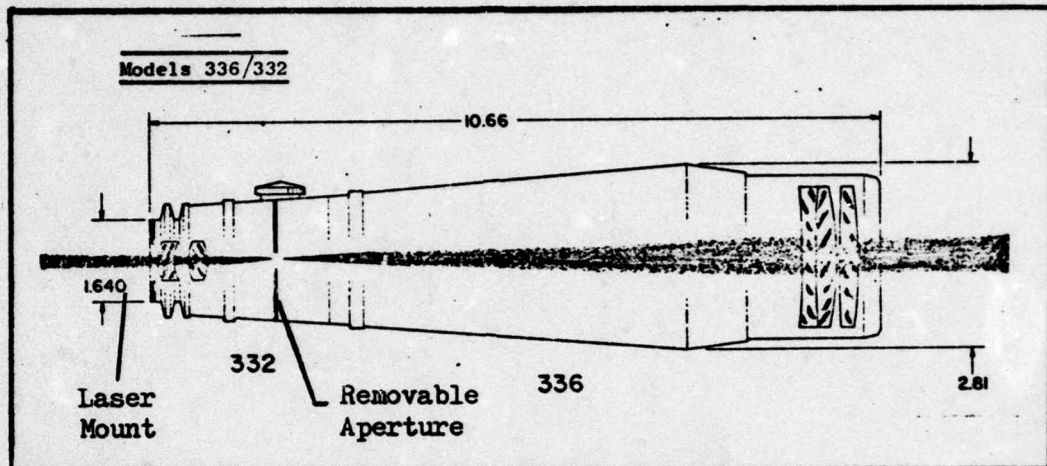


Fig. 9. Collimating Telescope

For operational testing using the 2.3 mw HeNe laser, the aperture was removed from the beam expander. This was necessary because the available aperture was too small, having been designed for use with a 50 mw laser. The wider beam coming from the larger laser could be focused onto a smaller aperture than could the 0.8 millimeter beam coming from the 2.3 mw laser. Laboratory tests showed that use of the aperture with the 2.3 mw laser would result in more than a 50% loss of power. Also, it was very difficult to produce a stable focus upon the aperture, resulting in power output instabilities. Elimination of the aperture produced a relatively stable beam and an output power of 2.12 mw, a power loss of only 10%.

A focusing ring on the aft portion of the collimator could be rotated to vary the position of the beam waist. Using the ring, it was possible to focus the beam within a few meters of the laser, or to produce the narrow downstream beam which was used during testing.

Table Mount. A stable platform was required on which the laser could be mounted. Also, since precise alignment of the laser was required, the mount had to be finely adjustable for tilt and azimuth.

The J. Unertl Optical Company mount, which was used, satisfied both of these requirements (See Fig. 9). Its heavy steel construction provided a support which was nearly free of vibrations, and large screw drives permitted precise tilt and azimuth control. The laser support was a 42 X 36 cm steel platform, which was suspended on a thick axle. Threaded holes around the perimeter of the platform could be used for locking the optical equipment in place. A third control permitted movement of the entire platform horizontally along the base of the mount. This type movement was used for alignment of the laser beam with the near end of the plastic safety pipe.

A 63 X 14 X 7 cm plexiglass block was used to elevate the laser above the platform of the mount. This additional elevation was needed so that the beam could clear a high balcony outside the tower window. The block was bolted to the platform, and the laser was bolted to the top of the block. A hole, which was drilled in the forward face of the block, held a support for the collimating telescope. A counterweight, which negated the downward tilt of the front end of the platform, was mounted in the aft face of the block. The rod along which the counterweight could be moved was 25 cm in length.

Safety Pipe. For safety reasons it was necessary to limit the area around the target in which the laser beam could fall. For this purpose a plastic pipe of inside diameter 5.5 cm was placed in front of the laser. The 3 meter long pipe allowed a field of view for the laser of approximately one degree around the target.

To insure rigidity, the pipe was securely mounted in a clamping device, which was attached to the balcony ledge of the tower (See Fig. 8). The pipe also tightly fit into a hole in a piece of plywood paneling, which had been mounted in place of the window glass.

Receiving Equipment

In the target plane a spherical mirror was used to capture the laser beam and focus it upon a power detector. Output of the detector was amplified and displayed on an XY recorder, which produced a log of each test run. The equipment is illustrated in Figure 11 and Figure 12 on the next page.

Mirror. The spherical mirror, which was used, had a concave, 31 cm diameter, front-coated surface. The quality of the surface was quite good, and a clean circular focus of collimated laser light could be obtained. The focused spot was approximately one millimeter in diameter and was located two meters from the mirror.

The mirror was attached to a heavy steel mount, which could be clamped to a table or a tripod. Tilt and azimuth controls on the mount produced movement of the mirror, and corresponding movement of the focused spot.

Laboratory and range testing showed that the mirror reflected $89 \pm 0.5\%$ of input collimated laser light onto the focal point. This figure was applicable to all portions of the mirror.

Detector. A Coherent Radiation power detector was positioned at the focal point of the mirror. The 1 cm^2 detector surface was uniformly sensitive to HeNe radiation, had a fast response time, and showed a linear response to input light intensity. A cylindrical light shield could be mounted on the detector housing to decrease background

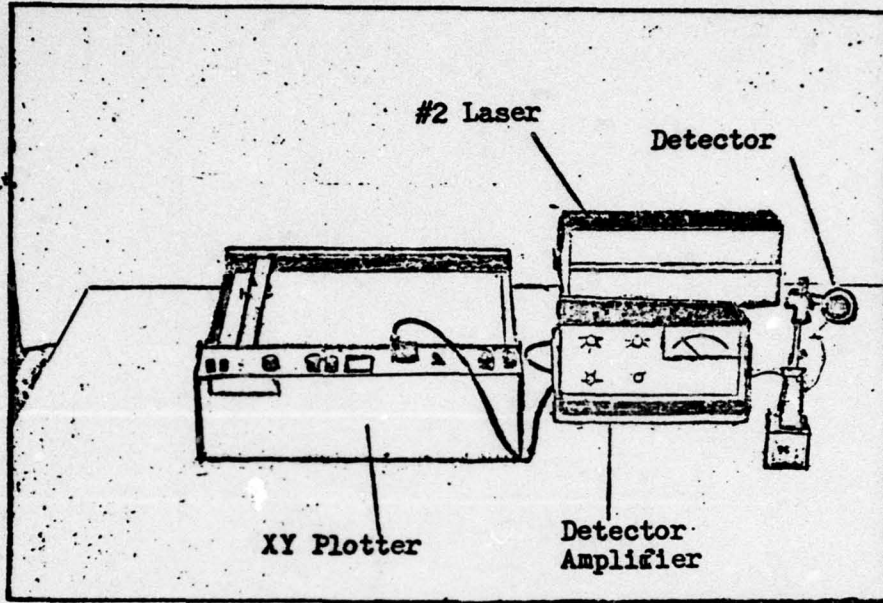


Fig. 10. Power Measuring Equipment

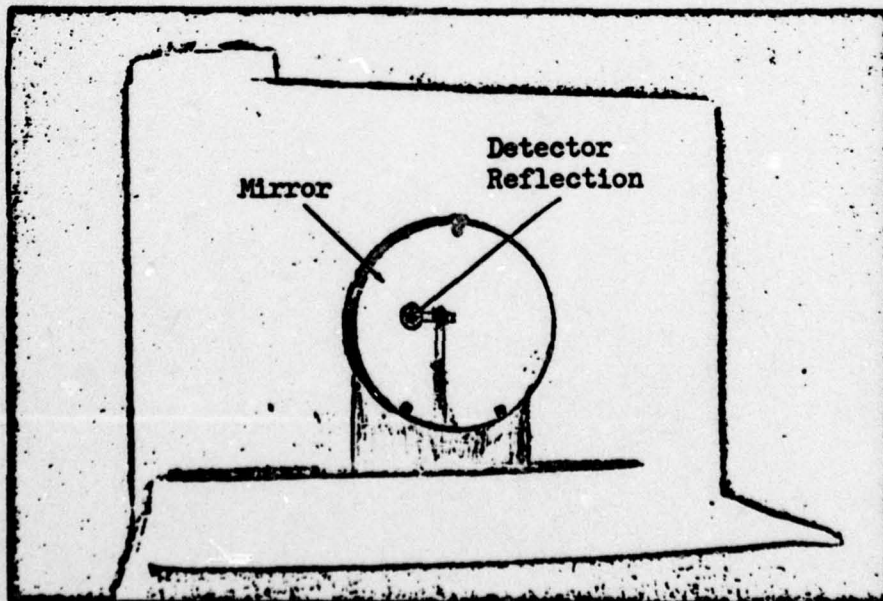


Fig. 11. Target Mirror

radiation, and a 1000/1 attenuator could be positioned in front of the detector if larger signals were to be measured.

The linearity of the detector was checked by placing neutral density filters between a test laser and the detector head. The filters transmitted a known fraction of the light which struck them. The detector produced power readings that were within 0.8% of predicted values when the beam was reduced in intensity to 10^{-3} , 10^{-5} , and 10^{-1} its original size.

The detector control unit contained a low voltage power supply, four 8.1 volt batteries. Detector readings were displayed on a self-contained meter and also could be output to a recording instrument. The range of possible full-scale readings on the meter was 0.1 microwatt up to 100 milliwatts (with the 1000/1 attenuator removed). An additional control was available for suppression of noise.

During initial laboratory testing the detector began to show large, random fluctuations in power indications, which were not caused by detected radiation. The fault was traced to two bad batteries in the control unit. Subsequent replacement of the batteries corrected the problem.

XY Recorder. Output of the Coherent Radiation detector was channeled to a Houston Instrument Model 2000 XY recorder. The Model 2000 had isolated and independent drive mechanisms for each axis. During the experiment, test runs were completed with the X axis drive in the automatic sweep, 10 sec/inch, position. Individual runs lasted approximately $2\frac{1}{2}$ minutes, using the full 15 inch X scale. Deflection of the recording pen along the Y axis was a function of input power from the detector. According to the instruction manual, the Y scale had a linearity $\pm 0.1\%$ of full scale. This linearity was verified at

the same time as was that of the power detector described in the last section.

The Y scale amplification control was set in the manual-adjust position. Then full scale deflection could be made to indicate 100% transmission from the transmitting laser. There also was a zero-set control for the Y scale. This control made it possible to set a convenient zero position for runs conducted under a variety of lighting conditions. Because of scale linearity, changing the zero position did not alter the scale difference between full scale and zero readings. This was verified during operation of the equipment.

Additional Equipment

In addition to equipment used for transmission and reception on the final range setup, other items were required during initial testing. A beam splitter and associated detection equipment were used during laboratory calibrations. Recalibration during range operation was accomplished with a second HeNe laser.

Beam Splitter. A beam splitter was used during initial calibration to reflect a portion of the beam leaving the collimating telescope onto a detector. In the lab it was then possible to simultaneously monitor laser output and power reaching the focal point of the spherical mirror. The source of any fluctuations or spurious signals could then be pinpointed.

The beam splitter was made from a glass, photographic plate, which measured 10 X 15 X 0.1 cm. The photographic coating had been removed by washing the plate with soap and water followed by an alcohol solution. Testing showed that the beam splitter reflected approximately 10% of laser light, which struck it at an angle of 30-50 degrees.

Detection Equipment Used with Beam Splitter. Light from the beam splitter was focused by a double-convex lens onto a SGD-040-A photodiode. The photodiode was operated in its conductive mode, producing current when stimulated by input light. According to EG&G Data Sheet D3003C-1, the detector output was linear within 1% over seven decades. The small size of the detector surface, 0.81 mm^2 , limited the usefulness of this detector. The laser beam had to be focused onto a very small spot, and any vibrations in the system produced an erratic signal. The detector, however, was adequate for laboratory calibrations.

The display unit utilized during calibration was a two-pen Honeywell XYY' recorder. The recorder received input from both transmission and reception equipment. The X drive of the recorder operated in an automatic sweep position. Separate amplification of each of the input signals was accomplished using the Y and Y' controls. Simultaneous recording of both laser output and downstream reception was then possible.

#2 HeNe Laser. A second HeNe laser was used to recalibrate reception equipment during range operation. The laser was the same model and had the same operating characteristics as did the primary laser. The only difference was that the #2 laser produced 1.48 milliwatts. The laser was used without a beam expander and collimator.

IV. Experimental Design and Operation

This chapter includes a description of the manner in which equipment was set up and used to obtain data during laboratory testing and initial range operation. Also, one section of the chapter contains a description of the physical characteristics of the range.

Laboratory Testing

Prior to range installation it was desirable to study all equipment under controlled laboratory conditions. In the lab the transmission and reception equipment could be separated by only a few meters, so that 100% transmission could be assumed. Losses of power could then be assigned to individual pieces of equipment. Also in the lab it was possible to try different configurations of equipment, and then decide upon the best arrangement. The following sections contain descriptions of the laboratory tests which were completed.

Telescope Alignment. As was mentioned in Chapter III, the diameter of the available aperture for the Model 332 beam expander was less than the optimum aperture size for the Model 132 laser. Therefore, the aperture was removed. Due to the amount of travel allowed by the beam expander mount, alignment of the laser beam with the beam expander longitudinal axis was difficult to accomplish. Central alignment was achieved by projecting the beam passing through the beam expander onto a white screen. The resulting pattern was a bright expanded laser spot within a larger, dim circle. The dim circle defined the possible transmission cone of the beam expander, and central alignment was completed by centering the laser spot. Then the collimator was attached to the beam expander. Downward tilt, caused by the additional weight,

was eliminated by placing a support under the forward end of the collimator. When the entire telescope was aligned, a uniform circular beam was projected onto the viewing screen.

Test of Laser Stability. Knowledge of laser output was the basis for all transmission measurements. Any existing power variations had to be documented as to size and frequency of occurrence. If the variations were small in comparison to detector resolution, continuous monitoring of laser output would not be required on the range. The presence of large fluctuations, however, would necessitate continuous monitoring.

Two methods were used to observe laser stability. The first, and simplest, was to focus the entire beam onto the Coherent Radiation detector. Focusing could be accomplished by adjusting the focus control on the collimator, or by reflecting the collimated beam from the spherical mirror. Output could then be read directly from the detector display or channeled to an XY recorder. The second method was to observe light reflected from a beamsplitter positioned just after the telescope. This was the method which necessarily would be used if continuous monitoring on the range was required.

Laboratory experimentation showed that when the laser was initially turned on, output fluctuations existed which had a magnitude of approximately 2% of total and a frequency of approximately 1/15 hertz. Tests demonstrated that the laser was solely responsible for these fluctuations, which existed immediately following laser turn-on, even if the other equipment was warm. As the laser warmed up the size of the fluctuations decreased and their frequency approached zero. After a warmup period of one hour, output was essentially constant. Therefore,

the laser could be used on the range without constant monitoring.

Classification of Optics. On the test range, percent transmission was calculated by comparing output power measurements, which were observed with identical equipment over short and long range lengths. Knowledge of the power losses associated with each piece of equipment was not required for these calculations. During planning and certain tests, however, it was desirable to know approximate, individual losses. These could be measured in the lab. The following is a list of such measurements:

- (1) Telescope - approximately 10% loss
- (2) Beam Splitter - approximately 10% loss
- (3) Spherical Mirror - approximately 11% loss

Comparison of #1 and #2 Lasers. For calibration purposes it was necessary to compare the power outputs of the primary laser and the #2 laser. This was done in two ways. In the first arrangement the primary laser beam was focused onto the detector. The resulting power measurement was compared to that from the #2 laser shining directly on the detector. In the second arrangement the spherical mirror was used to focus the collimated primary beam and then the #2 beam onto the detector. This arrangement duplicated the range setup, except for the proximity of the laser and mirror. The ratio of power outputs in both test arrangements was $69.6 \pm 0.2\%$. This figure was used for subsequent calibrations using the #2 laser.

Field Calibrations

The range receiver consisted of the spherical mirror which reflected light onto the detector, which in turn, produced a deflection on the Y scale of the XY recorder. Final results for each test run were calculated

by comparing the observed scale deflection to the scale deflection associated with 100% transmission. Originally this 100% power indication was obtained, as mentioned in the last section, by placing the primary laser within a few meters of the mirror. Full scale deflection, corresponding to 100% transmission, was manually set at 9 inches. Subsequent scale readings were compared to this standard.

After all transmission and reception equipment had been installed on the range, it was impractical to recalibrate daily by taking a short-distance reading with the primary laser. For that reason, the #2 laser was used to recheck calibration. It was placed a few meters in front of the mirror, and the observed scale deflection, which resulted, was checked to correspond to $(9 \text{ inches}) \times (0.696) = 6.3 \text{ inches}$. Only minor adjustments of less than 0.1 inch were required on any such recalibration.

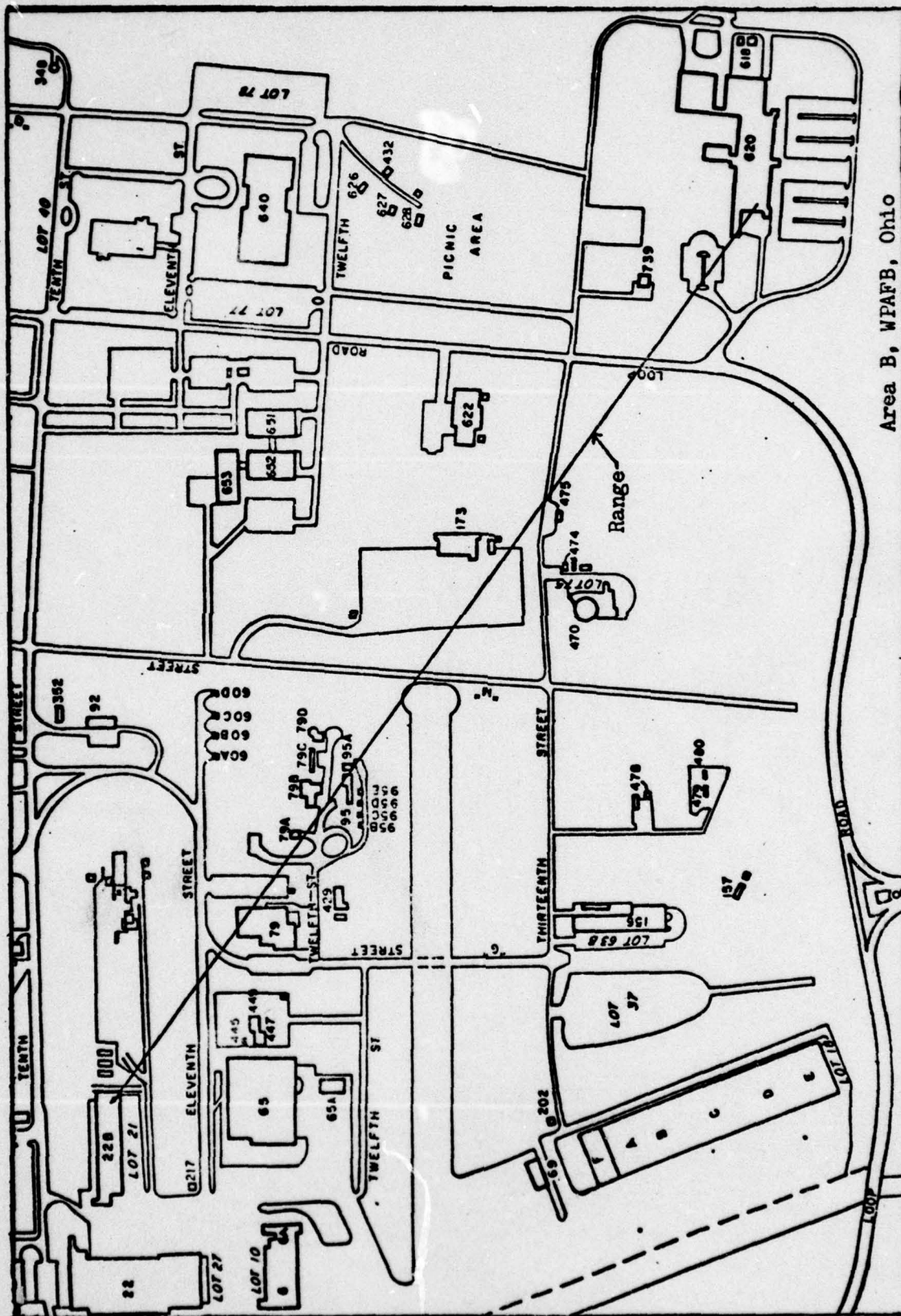
Once during the tests the mirror was taken to the transmitter in the tower so that another short-range calibration could be made with the primary laser. The mirror was clamped to a tripod and positioned on the balcony in front of the undisturbed laser. This calibration agreed to within 0.4% of previous short-range calibrations.

A Range Description

The optical range was set up in Area B of Wright Patterson AFB, Ohio. Experiments were conducted over an open-air path from the transmitter in Building 620 to the receiver in the penthouse of Building 22B.

An overhead depiction of the range is given in Figure 13. The length of the optical path was 4040 feet or 1.23 km. A vertical profile graph is given in Figure 14, and as can be seen from the diagram, the vertical drop along the range was approximately 300 feet (90 meters). The average

BEST AVAILABLE COPY



Area B, WPAFB, Ohio

Fig. 12. Overhead Diagram of Range

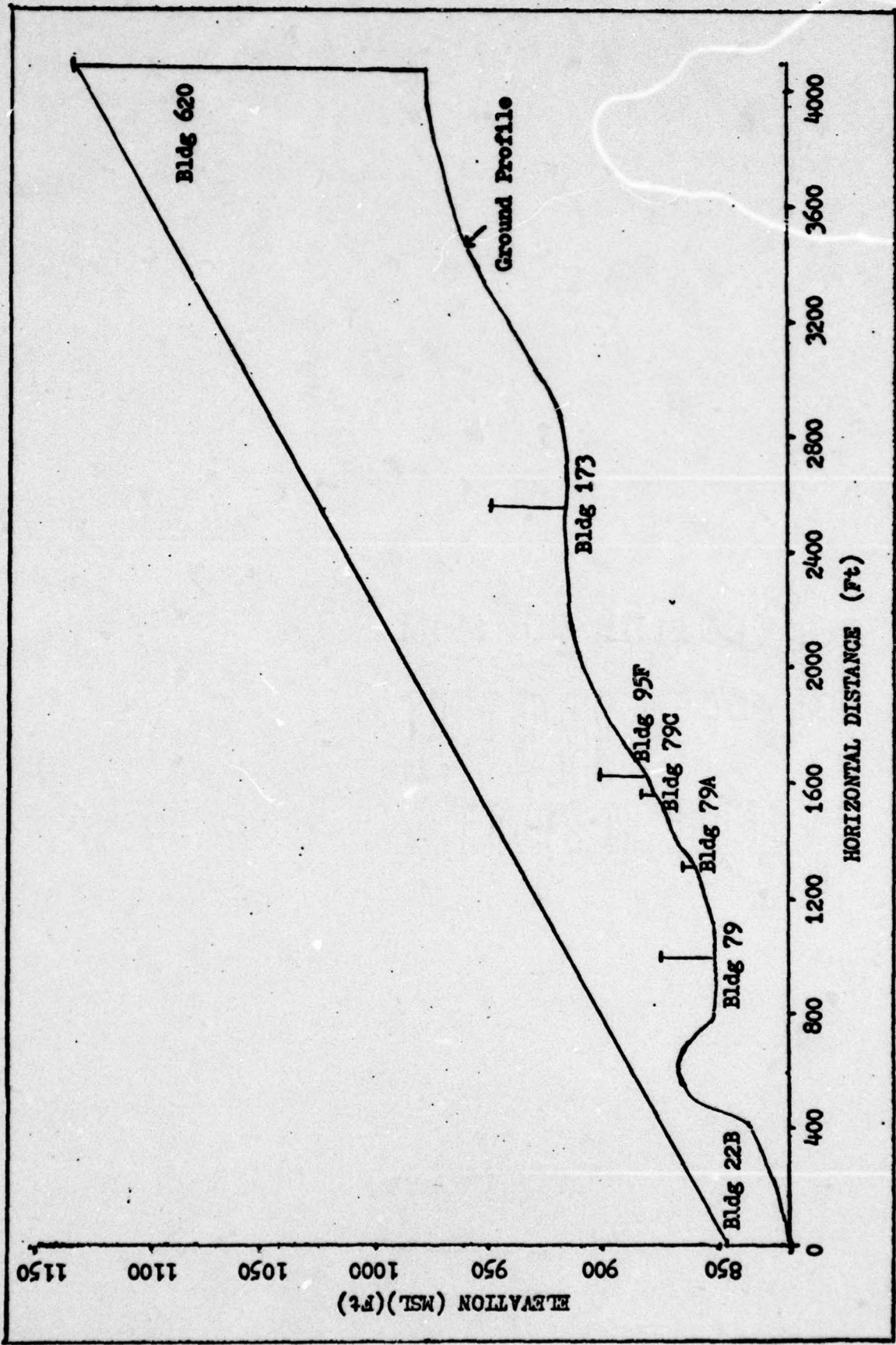


Fig. 13. Vertical Diagram of Range

altitude was approximately 1000 feet (305 meters) MSL, and the average height above the ground was 100 feet (30 meters).

Figure 15 is a view of the penthouse as seen from the transmitter. The penthouse window is at the center of the picture. Figure 16 is a view of the tower as seen from the receiver. The transmitter was located on the 11th floor of the tower, two stories down from the top. Figure 17 is a blowup of the view given in Figure 15. The maximum field of view (FOV) of the laser, as restricted by the safety pipe, is depicted on this blowup. As is indicated, the maximum FOV was approximately one degree. The ridgeline, which is prominent in Figures 15-17, can also be found on the vertical profile diagram (Fig. 14). It was located approximately 500 feet (102 meters) along the line of sight from the receiver. The top of the ridge was approximately 30 feet (9 meters) below the line of sight.

Equipment Alignment

After transmitting and receiving equipment were in place at either end of the range, alignment of the laser beam with the receiver was accomplished.

Field of View Adjustment. The first step in alignment was to adjust the plastic safety pipe so that the target was centered in its field of view. This was accomplished by sighting down the interior of the pipe. Thereafter, when the laser passed through the pipe, it was roughly aligned within one degree of the target (see Fig. 17).

Nighttime Alignment. Final alignment could most easily be achieved under conditions of darkness. The nearly collimated laser beam at night looked like a spotlight beam when viewed from the target. The observer could easily give telephone directions for centering the beam within the

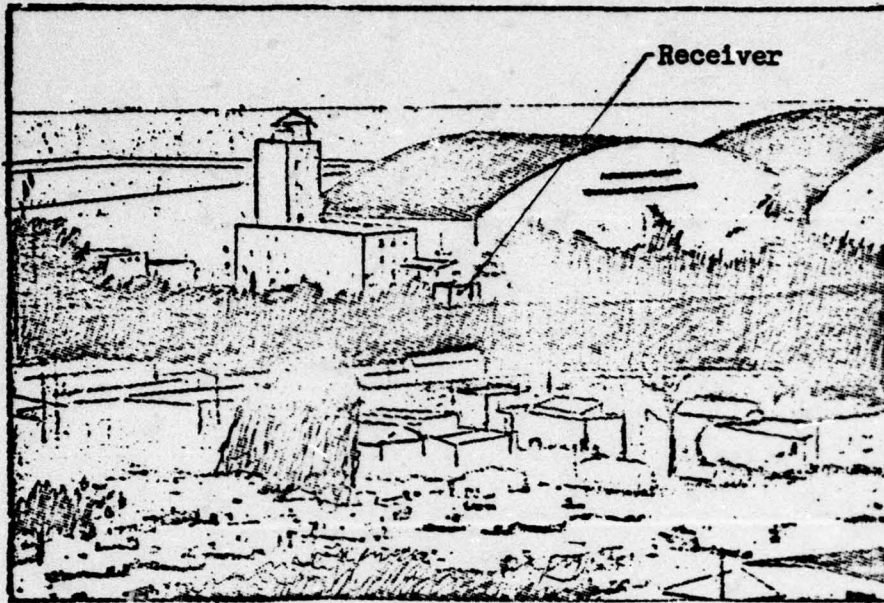


Fig. 14. View of Bldg 22B Penthouse from Bldg 620 Tower

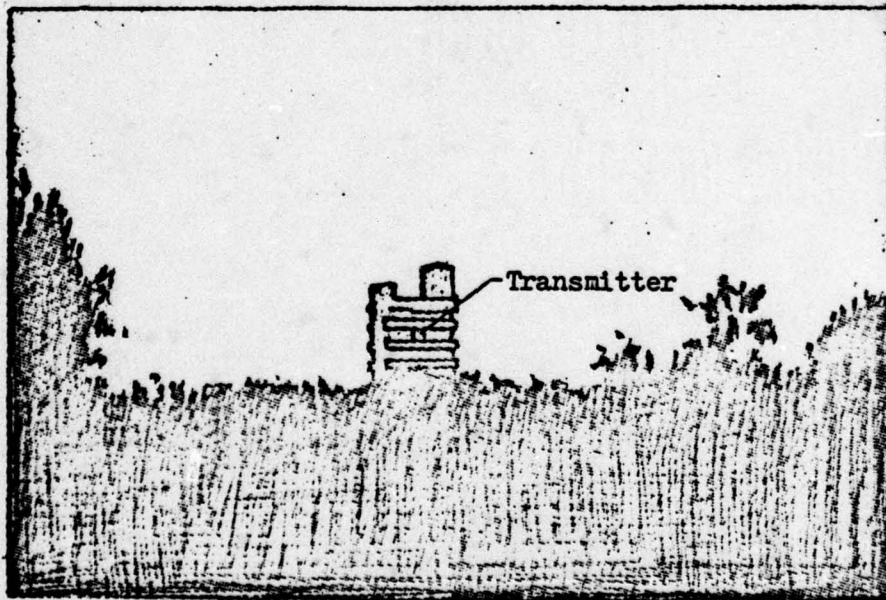


Fig. 15. View of Bldg 620 Tower from Bldg 22B Penthouse

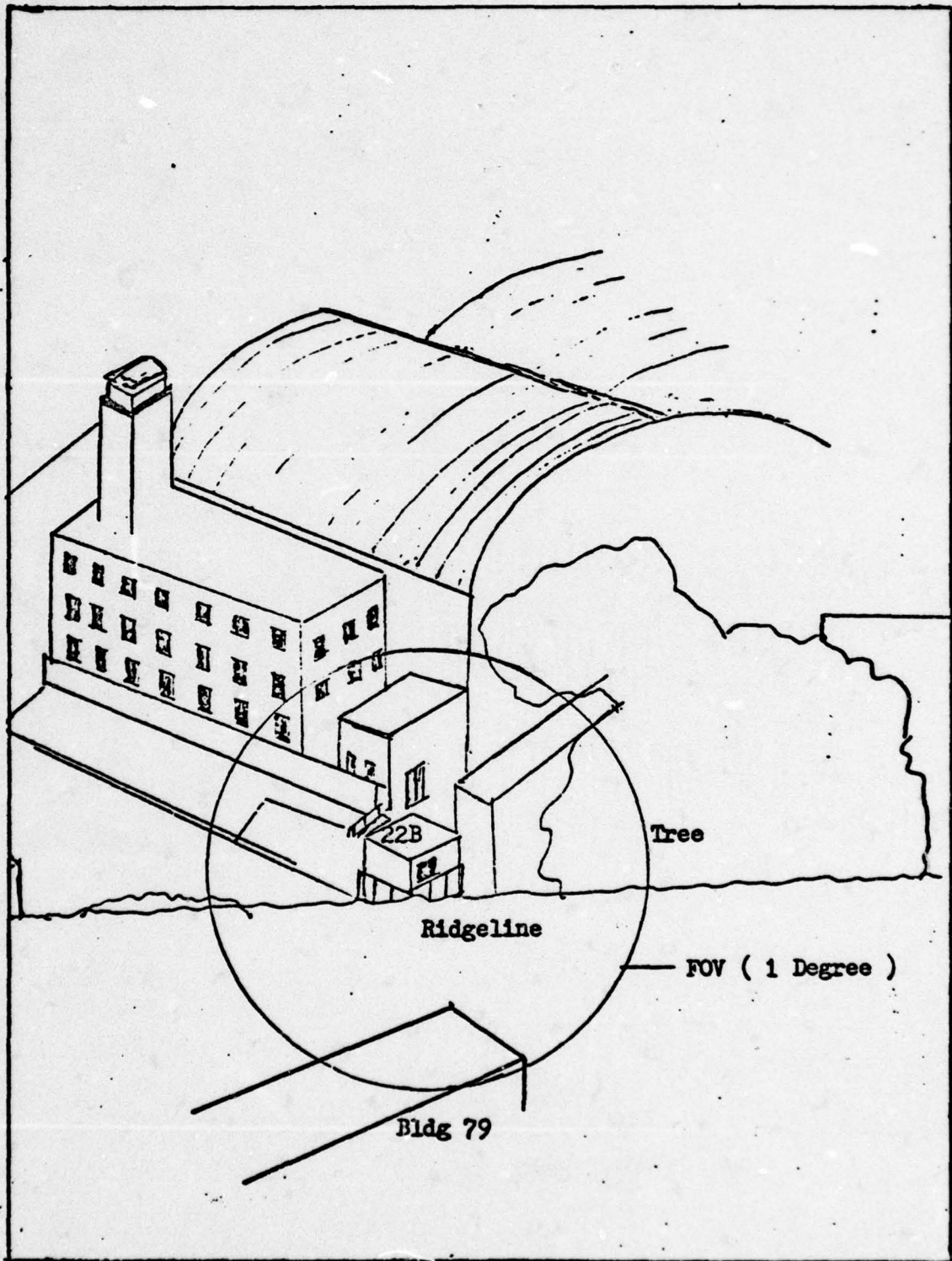


Fig. 16. Blowup of Fig. 15 Showing Maximum Field of View

empty, penthouse window. Directions from the observer were followed at the transmitter by making minor adjustments of the tilt and azimuth controls of the table mount. After the laser beam was aligned, the safety pipe was adjusted so that the beam passed along its central axis. Next, the beam collimation was tested by making minor adjustments of the telescope focusing ring. The smallest possible beam at the target plane was desired. Focus adjustments either side of this collimated position produced an enlarged spot size.

Nighttime alignment was easy to accomplish, but test runs were to be completed during daylight hours when visibility estimates could be made. Therefore, since alignment proved to be unstable, it was necessary to develop a technique for daytime alignment.

Daytime Alignment. Final alignment during daytime conditions was difficult to accomplish. The nearly collimated beam could not be seen from the penthouse unless it was within one or two meters of the window. The solution to this problem was to defocus the beam so that a larger spot reached the target plane. This larger spot could be more easily seen. When the beam was judged to be centered in the window, a small adjustment in focus of the telescope, toward collimation, was made. After many small center-and-focus adjustments were accomplished, it was possible to align the collimated beam within the window.

Beam Drift. Daily alignment was required due to the beam drift which was encountered. For a period of several hours after laser turn-on, the beam always dropped. This happened both at day and at night. The sink rate was initially quite large, approximately 12 cm/5 minutes. After four or five hours the beam stabilized, and then reversed directions. The upward drift rate was slow and was never observed for more than eight hours after turn-on. No lateral drift was ever observed.

Overnight the alignment was always left at its last in-window position. Normally this was the raised position associated with the warm laser. Each morning when the laser was turned on, the beam initially was high. Apparently the alignment had returned to the cold laser position.

The reason for the beam drift was not discovered. The most likely cause was heat deformation of interior optical components of the laser. An attempt to cure a less likely cause, movement of the table mount, was made by attaching a counterweight to the rear of the plexiglass, laser support. This attempt was not successful.

The beam drift was annoying, but transmission measurements could still be made. The target mirror was clamped to a moveable table and was repositioned within the penthouse room to catch the beam. Movement of the detector was also required.

Test Run Procedures

Each test run was accomplished by completing a standard set of operating procedures. The separate procedural steps are described in this section.

Warmup Period. All equipment, including the #2 laser, was turned on at the start of each day. A minimum of one hour warmup preceded the first test run. During this period the transmitter beam was not allowed to exit the tower.

Recalibration. Each day after the equipment was warm the #2 laser was used to check calibration of the XY recorder. Only minor adjustments of the Y scale were ever required. The calibration also included adjustment of the zero scale position. As was mentioned in the description of the XY recorder, movement of the zero position did not alter the scale difference between zero and full scale readings.

Realignment. As was mentioned earlier, the laser beam tended to drift downward as the laser warmed up. Therefore, it was necessary each day to align the laser within the target window. Final centering of the beam upon the mirror was achieved by moving the mirror. When the mirror was moved, the detector had to be repositioned at the new focal point.

Weather Observations. Prevailing weather conditions were recorded at the time of each test run. Recorded data included temperature, dew point, barometric pressure, winds, and visibility. The base weather shop was the source of all weather data except prevailing visibility. Estimates of visibility were made by observation from the tower. An enlarged version of Figure 18 served as a reference for those estimates.

Transmission Measurement. With the beam on target and all reception equipment operational, a test run could be accomplished. Using the sweep position of the recorder, normally a $2\frac{1}{2}$ minute sample was taken. During the run the zero scale position was established by blocking for a short period the beam between the mirror and the detector. This technique produced the same results as were obtained by blocking the beam at the transmitter.

Percent transmission was calculated by comparing the average scale reading during the run to the standard 9 inch figure for 100% transmission. The range of scale readings during test runs was never observed to vary more than 2% from the mean.

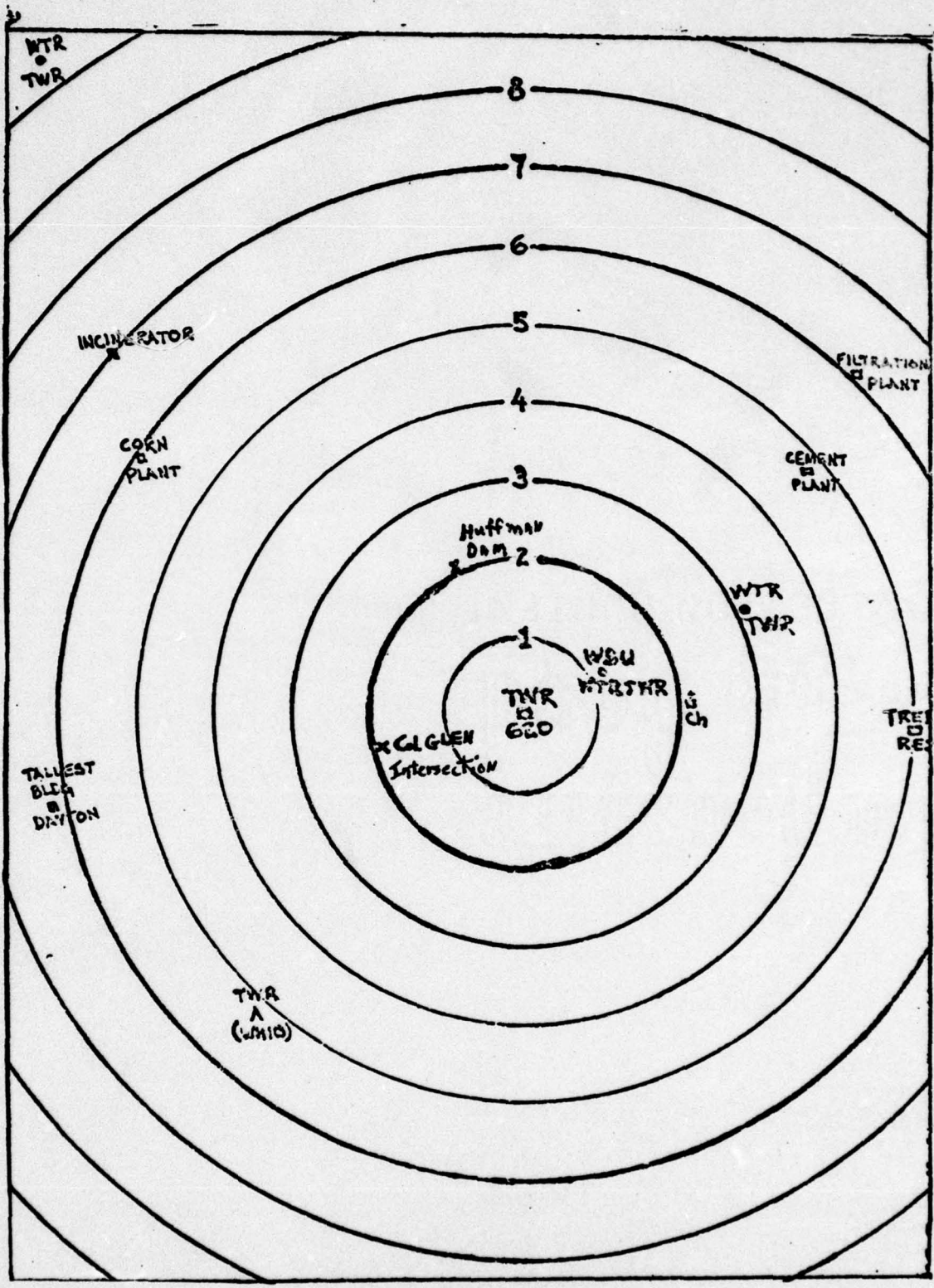


Fig. 17. Visible Range of Prominent Local Features As Viewed From the Tower of Bldg 620

V. Experimental Results and Data Analysis

The equipment on the range operated successfully. Results of preliminary testing have been given in descriptions of equipment and range design in earlier chapters. This chapter includes a discussion of the transmission measurements which were made, and a description of the atmospheric turbulence effects which were observed.

Transmission Measurements

Transmission measurements were made on 20 occasions over a period of two weeks. A longer period of testing had been planned, but a delay was encountered. Safety approval for open-air testing could not be obtained until approximately two months after the study began. Fortunately, during the time which was available for testing a large variety of weather conditions could be observed. Test runs were completed during periods when the visibility ranged from 2 km to 18 km. The results of the test runs and a description of prevailing weather conditions during each run are included in Table IV.

A comparison of experimental results and theoretical predictions is depicted in Figure 19. The theory behind such comparisons was presented under "Aerosol Attenuation" in Chapter II. As can be seen in the diagram, the agreement was good. This implies that the HeNe, low-level attenuation coefficients, as given by McClatchey and Selby, were accurate when applied in the manner discussed in Chapter II. The technique, which was used to interpolate between aerosol coefficients for a "clear" and a "hazy" day, provided theoretical predictions which closely agreed with test results.

Values for percent transmission are assumed to be correct to within

TABLE IV

TEST RUN DATA

Test Run	Temp (C)	Dew Point (C)	Pressure (mb)	Winds (mph)	Visibility (km)	Percent Transmission
1	21	20	993	170/2	5.6	67.0
2	24	21	993	190/3	6.5	69.4
3	28	22	992	210/8	11.2	80.5
4	32	21	991	200/6	9.5	75.0
5	24	22	994	190/2	4.0	57.8
6	26	22	994	240/4	6.5	67.0
7	30	22	994	270/8	9.5	74.4
8	32	19	993	250/8	11.2	79.4
9	24	22	993	150/3	3.2	46.6
10	26	22	993	210/2	4.0	53.3
11	29	21	993	220/6	8.0	72.7
12	22	20	988	090/4	2.0	36.6
13	21	17	990	070/2	4.8	65.5
14	22	18	990	020/3	5.6	66.1
15	26	19	990	030/2	5.6	64.4
16	16	14	990	030/1	9.6	72.2
17	19	14	990	040/4	16.1	85.0
18	24	16	990	040/6	17.7	86.1
19	26	17	990	040/6	16.1	83.9
20	20	18	988	200/5	3.2	45.0

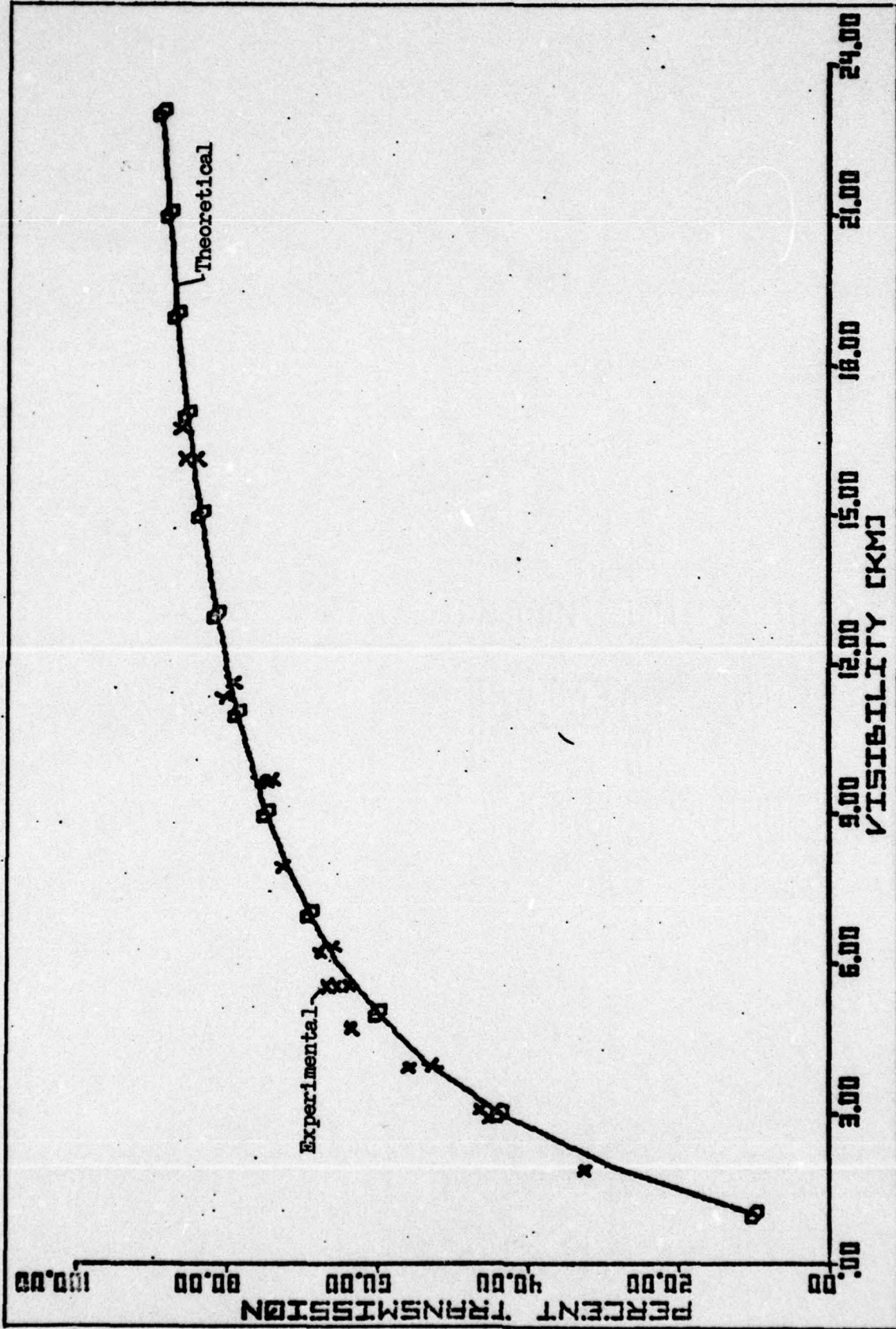


Fig. 18. Comparison of Experimental and Theoretical results for HeNe Laser
(Percent Transmission versus Visibility)

3.0%. This figure takes into account errors associated with power fluctuations, mistakes in calibration, and attenuation changes which occurred during the test run (see Appendix D).

The major source of error during these experiments was the imprecision associated with prevailing visibility estimations. Observations from the tower were the most reliable, but these estimates could be assumed correct only to within 20%. The short distance estimates were the most accurate. This was fortunate since the rate of change of attenuation coefficients was most rapid under reduced visibility conditions.

Turbulence Effects

Each of the turbulence effects mentioned in Chapter II was observed during test runs. These included spot dancing, beam spreading, image dancing, and scintillation. Because the mirror surface was much larger than the projected beam, turbulence had little or no effect upon transmission measurements.

Spot Dancing. The amount of spot dancing which was observed varied from less than 1 cm under non-turbulent conditions to approximately 5 cm during strong turbulence. Due to the amount of scintillation normally present, accurate measurement of the amount of spot dancing was not easily accomplished.

Beam Spreading. The diameter of the laser spot upon the target plane was constantly changing. The rate and magnitude of the changes was directly related to the amount of turbulence present. During strong turbulence beam diameter fluctuated by as much as 30%. During calm conditions only minor spreading was apparent.

Image Dancing. A small amount of image dancing was observed. The focused spot moved less than 1 millimeter upon the detector under the worst conditions. This movement had no effect upon measurements taken with the Coherent Radiation detector, which had a sensitive surface of over 1 cm². There was, however, too much movement to permit the use at the receiver of the photodiode detector, which had a smaller surface area.

Scintillation. Image breakup, due to scintillation, was always present to some degree during test runs. The effect produced constant movement of bright and dark areas within the projected spot. During calm conditions the observed intensity pattern closely resembled photograph (a) of Figure 6. During strong turbulence the pattern looked much like (b) of Figure 6 (page 25).

VI. Conclusions and Recommendations

The purpose of this research was to establish an optical range and use it to study atmospheric attenuation of laser radiation. The range was set up in Area B of Wright Patterson AFB, Ohio. The length of the open-air course was 1.23 km, and the average height above the ground was 30 meters. Initial testing was completed using a HeNe laser. Eventually other lasers, in particular the CO₂ laser, will be tested on this, or a similar range.

Conclusions

Atmospheric attenuation of a low powered HeNe laser beam was examined both theoretically and experimentally. Experimental results were limited, but useful information could be extracted from the data. Close agreement was found between experimental results and theoretical predictions. The theoretical predictions were based on interpolation between aerosol attenuation coefficients as given by McClatchey and Selby for two visibility models (Ref 9)(Table I).

The effects of atmospheric turbulence upon laser propagation were also examined. During this stage of testing an attempt was made to minimize the effect turbulence had upon test results. The conclusion of a theoretical study was that by using a receiver several times larger than the expected beam size at the target, it would be possible to accomplish this reduction. The prediction proved true during test runs. In later experiments, more time will possibly be devoted to study of the effect turbulence has upon laser propagation. If the receiver in future tests is smaller than the target spot size, turbulence may have a great effect upon observed transmission measurements.

Recommendations

In the limited number of test samples which were taken, observed attenuation of HeNe radiation was of the expected magnitude. Attenuation predictions for lasers operating in the infra-red portion of the spectrum, however, may not prove to be as reliable. Other lasers, particularly the CO₂ laser, need to be tested under a variety of well documented weather conditions.

Concurrent Testing. An ideal arrangement would be to conduct concurrent testing of a CO₂ laser and a Yag laser. Theoretically the CO₂ laser radiation should be less effected by low visibility. Concurrent testing would permit direct comparison of the two lasers under a variety of weather conditions.

Visibility Measurements. During initial test runs, estimates of prevailing visibility were made by observation of local landmarks from the tower of Building 620. These estimations played an important role in the interpretation of test data. In later tests a more objective method of measuring visibility should be found. Possibly an instrument for measuring visibility will be operational in the tower of Building 620 prior to future experimentation. Also, consideration should be given to the idea of concurrently operating a HeNe laser as a transmission reference in the visible portion of the light spectrum.

Future Test Approval. An approval must be obtained for each laser which is to be tested. Due to the delay that can be expected, a request for approval should be submitted at least six months prior to the desired test date. The test designer should be aware that restrictions will probably be placed on the size and type of laser which can be used, and on the operating procedures that must be followed during experimentation.

Joint Research Project. If this research is continued by AFIT, it would be advisable to have the project shared by at least two students. Operation of the range cannot be efficiently accomplished by one student, since personnel are required at each end of the range. Another alternative would be to assign a student to an ongoing research effort supported by other base organizations.

Bibliography

1. AFM-161-32. Laser Health Hazards Control. Washington: Department of the Air Force, April 1973.
2. AMC Pamphlet AMCP 706-127. Infrared Military Systems, Part One: Alexander, Virginia: Department of the Army, May 1973.
3. Chiba, T. "Spot Dancing of the Laser Beam Propagated through the Turbulent Atmosphere." Applied Optics, 10: 2456-2461 (1971).
4. Davis, J. I. "Consideration of Atmospheric Turbulence in Laser Systems Design." Paper presented at the Conference on Atmospheric Limitation to Optical Propagation, Boulder Colorado, 17 March 1965.
5. Gilmartin, T. J. and J. Z. Holtz. "Focused Beam and Atmospheric Coherence Measurement at 10.6 μm and .63 μm ." Applied Optics, 13: 1906-1912 (1974).
6. Kondratyev, K. YA. Radiation in the Atmosphere. New York: Academic Press, 1969.
7. McClatchey, R. A. and J. E. A. Selby. Atmospheric Attenuation of Laser Radiation From 0.76 to 31.25 μm , AFCRL-TR-74-0003, 3 January 1974.
8. -----, Atmospheric Transmittance, 7-30 μm : Attenuation of CO₂ Laser Radiation, AFCRL-72-0611, 12 October 1972.
9. -----, Optical Properties of the Atmosphere, AFCRL-70-0527, 22 September 1970.
10. Middleton, W. E. K. "The Effect of the Angular Aperture of the Telephotometer on the Telephotometry of Collimated and Noncollimated Beams." Journal of the Optical Society of America, 39: 573-578 (1949).
11. Mie, G. "Beitrage zur Optik Truber Medien, Speziell Kolloidaller Metallosungen." Annalen der Physik, 25: 377-445 (1908).
12. Raidt, H. "Propagation of Focused Laser Beam in the Turbulent Atmosphere." in AGARD-CP-183, 21, May 1976.
13. Siegman, A. E. An Introduction To Lasers and Masers. New York: McGraw-Hill, Inc., 1971.
14. Shettle, E. P. and R. W. Fenn. "Models of the Atmospheric Aerosols and Their Optical Properties." in AGARD-CP-183, 2, May 1976.
15. SPA 332/333/334/336. Models 332/333/334/336 Instruction Manual. Mountain View, California: Spectra-Physics, Inc., Jul 1969.

16. Van de Hulst, H. C. Light Scattering by Small Particles. New York: John Wiley and Sons, Inc., 1957.
17. Wright P. J. "A Comparative Study of Atmospheric Transmission at Three Laser Wavelengths in Relation to the Meteorological Parameters." in AGARD-CP-183, 3, May 1976.
18. Zajac, A. and E. Hecht. Optics. Reading, Massachusetts: Addison-Wesley Publishing Company, Inc., 1975.

Appendix A

Standard Operating Procedures (SOP) for Outdoor Testing of Open-Air Lasers

Prior to Turn On

1. All personnel will be familiar with the following:
 - (a) AFM 161-32 (Revised)
 - (b) AFM 127-101
 - (c) AFR 161-24
 - (d) T.O. 00-25-247
 - (e) General safety precautions which are to be followed
2. Manufacturer's operating procedures of the specific laser being used will be reviewed.
3. All personnel will be made aware of existing electrical hazards.
4. SEED calculations for the test laser will be completed in accordance with AFM 161-32 (Revised).
5. The beam path should be line of sight clear. A vertical profile of the path of the laser beam will be drawn to insure clear line of sight. The beam will originate and end within a secured area.
6. Arrangements will be made for proper termination of the beam, making sure that no specular reflections will occur.
7. All personnel will wear correct eye protection for the laser being used.
8. If the laser malfunctions or is move accidentally, it will be turned off immediately and the remaining personnel informed of the problem.
9. During communication between test sites, proper RTO procedures will be followed.
10. Besides having a person in charge of the experiment, a Safety Officer

will also be appointed. He will have supreme veto power over any command if an unsafe condition exists. He will also watch the path of the laser beam to see that it is clear of personnel.

11. Care should be taken to insure all equipment being used is mounted securely.

12. No less than two people will be with the laser at all times.

13. A mask will be constructed in front of the laser with a hole cut out to limit the angle of travel if the laser should be accidentally bumped or jolted.

14. To provide a controlled area, laser warning signs will be placed in the following positions: (a) on the inside of the stairway door, (b) on the inside of the elevator door.

15. A set of Operating Instructions will be written for every test or series of tests to be conducted. Included will be the following:

- (a) This SOP
- (b) Drawings, charts, and calculations with stated assumptions
- (c) Hours of operation
- (d) List of persons in charge
- (e) A Total Hazard Analysis containing, but not limited to, assessment of possible electrical and physical hazards.

16. Coordination through the following offices will be initiated before commencing tests:

- (a) Laboratory Safety Administrator, AFAL/TSS-1
- (b) AFWAL/SE
- (c) MED CEN/SGPB
- (d) 2750th/SEG
- (e) 2750th/OT

Written operating instructions will be sent to each of the listed offices for coordination with approval coming from 2750th/CC.

Turn On Procedures

1. When the laser is set up and ready to be turned on, all personnel in the test site will be notified. The laser will be turned on after this notification has been acknowledged.
2. Initial alignment of the HeNe laser will be accomplished with the aid of a person in the penthouse of Building 22B. This person will be in telephone communication with the transmitting site.
3. Penthouse personnel will not look directly back at the output of the laser with the naked eye.

Turn Off Procedures

1. The laser will be turned off in accordance with the manufacturer's operating procedures.
2. All personnel will acknowledge the laser has been turned off.
3. If terminating test for the day, the test site will be cleaned before leaving.

Exposure

If human exposure to laser energies greater than the PEL occurs, the following steps will be taken:

- (a) Medical treatment will immediately be obtained
- (b) MEC CEN/SGB will be contacted
- (c) Information required for a written report per AFR 161-24 will be obtained

Visitors

Visitors are AFAL or AFIT personnel who are not participating in or directly involved with the experiment being conducted. Visitors will comply with the following:

- (a) Be verbally briefed on what they are about to witness and alerted to all potential dangers
- (b) Read the SOP
- (c) Wear proper eye protection for the laser being used
- (d) Be subject to the same regulations and SOP as the operators
- (e) Not be allowed to operate the laser

Appendix B

Radiation Hazard Evaluation For HeNe Laser

SEED Calculations (Ref 1)

- (a) Time Limitation = 8 hr = 2.88×10^4 sec
- (b) Laser Power = 2×10^{-3} watts
- (c) Beam Diameter = 3 cm
- (d) Beam Divergence = 3×10^{-5} radians
- (e) Effective Energy = $Q = (2\text{mw})(2.88 \times 10^4 \text{sec}) \frac{(\pi/4)(.7\text{cm})^2}{(\pi/4)(3 \text{cm})^2} = 3.13 \text{ j}$
- (f) Radiant Exposure = $H = Q (\pi/4 (.7\text{cm})^2)^{-1} = 8.14 \text{ j/cm}^2$
- (g) Ocular MPE = $17.58 \times t \times 10^{-6} = .506 \text{ j/cm}^2$
- (h) Skin MPE = $0.2 t = 5.76 \times 10^3 \text{ j/cm}^2$
- (i) Ocular SEED = $\left[\left(\frac{4 Q}{\pi \text{MPE}} \right)^{\frac{1}{2}} - 3 \text{ cm} \right] / 3 \times 10^{-5} \text{ rad} = -6.4 \times 10^1 \text{ meters}$
- (j) Skin SEED = 0 meters (H less than Skin MPE)

The energy density calculations for the HeNe laser, which are given above, show that for the worst-case condition of continuous eight hour operation, both the ocular SEED and the skin SEED are 0 meters. Thus the laser radiation hazard is negligible everywhere.

Appendix C

Radiation Hazard Evaluations For CO₂ Lasers

SEED Calculations for Noncollimated Beam (Ref 1)

- (a) Time Limitation = 8 hr = 2.88×10^4 sec
- (b) Laser Power = 5 watts
- (c) Beam Diameter = 0.5 cm
- (d) Beam Divergence = 3.5×10^{-3} radians
- (e) Effective Energy = $Q = (5 \text{ watts})(2.88 \times 10^4 \text{ sec}) = 1.44 \times 10^5 \text{ j}$
- (f) Ocular and Skin MPE = $0.1 \times t = 2.88 \times 10^3 \text{ j/cm}^2$
- (g) Ocular and Skin SEED = $\left[\frac{4Q}{\pi \text{ MPE}} \right]^{\frac{1}{2}} - .5 \text{ cm} \Big] / 3.5 \times 10^{-3} \text{ rad} = 21.4 \text{ m}$

SEED Calculations for Collimated Beam (Ref 1)

- (a) Time Limitation = 2.88×10^4 sec
- (b) Laser Power = 5 watts
- (c) Beam Diameter = 5 cm
- (d) Beam Divergence = 1×10^{-4} radians
- (e) Effective Energy = $Q = (5 \text{ w})(t) \frac{(\pi/4)(.7)^2}{(\pi/4)(5)^2} = 2.82 \times 10^3 \text{ j}$
- (f) Ocular and Skin MPE = $0.1 \times t = 2.88 \times 10^3 \text{ j/cm}^2$
- (g) Ocular and Skin SEED = $\left[\frac{4Q}{\pi \text{ MPE}} \right]^{\frac{1}{2}} - 5 \text{ cm} \Big] / 1 \times 10^{-4} \text{ rad} = -3.88 \times 10^2 \text{ m}$

Appendix D

Error Analysis for Experimental Results

The equation for calculating percent transmission is:

$$\%T = a/b \quad (13)$$

where: $a = 4$ to 8 inches ± 0.2 inches (XY Plotter Scale Deflection)

$b = 9.0 \pm 0.2$ inches (Full Scale Deflection)

The equation for calculating the standard deviation in transmission measurements is:

$$S_t = (\%T) \{ (S_a/a)^2 + (S_b/b)^2 \}^{1/2} \quad (14)$$

For $\%T = 90\%$

$$S_t = (.90) \{ (.2/8.1)^2 + (.2/9.0)^2 \}^{1/2} = 2.8\%$$

For $\%T = 40\%$

$$S_t = (.40) \{ (.2/3.6)^2 + (.2/9.0)^2 \}^{1/2} = 2.4\%$$

where:

S_a includes:

Scale variation during $2\frac{1}{2}$ minute run = ± 0.2 inches

S_b includes:

XY Plotter Linearity = $\pm 0.1\%$ (p33)

#1/#2 Laser Power Ratios = $\pm 0.2\%$ (p38)

Max Recal. Adjustment
Using #2 Laser = $\pm 1.1\% = .1/9$ in (p39)

Max Recal. Adjustment
Using #1 Laser = $\pm 0.4\%$ (p39)

Total = $\pm 1.8\%$ or 0.2 inches on 9.0 scale

Vita

Graham Gilmer Williford was born 11 November 1946 in Richlands, Virginia. He attended King College in Bristol, Tennessee, and graduated in 1968 with a B.A. in Physics. After receiving an Air Force commission from OTS, he completed Undergraduate Pilot Training at Williams AFB, Arizona. His first assignment after UPT was as an OV-10 FAC in Southeast Asia. Upon returning in 1971 he was assigned as an instructor pilot in the T-38 aircraft at Craig AFB, Alabama. After two years at Craig AFB he was assigned as an instructor pilot at Pilot Instructor Training School at Randolph AFB, Texas. He entered the Air Force Institute of Technology in June 1976.

Permanent address: 215 Wyanoke Drive
San Antonio, Texas 78209

Unclassified

SECURITY CLASSIFICATION OF THIS PAGE (When Data Entered)

REPORT DOCUMENTATION PAGE		READ INSTRUCTIONS BEFORE COMPLETING FORM
1. REPORT NUMBER GEP/PH/77-17	2. GOVT ACCESSION NO.	3. RECIPIENT'S CATALOG NUMBER
4. TITLE (and Subtitle) ATMOSPHERIC ATTENUATION OF HeNe LASER RADIATION		5. TYPE OF REPORT & PERIOD COVERED MS Thesis
		6. PERFORMING ORG. REPORT NUMBER
7. AUTHOR(s) Graham G. Williford Capt, USAF		8. CONTRACT OR GRANT NUMBER(s)
9. PERFORMING ORGANIZATION NAME AND ADDRESS Air Force Institute of Technology (ENP) Wright-Patterson AFB, Ohio 45431		10. PROGRAM ELEMENT, PROJECT, TASK AREA & WORK UNIT NUMBERS
11. CONTROLLING OFFICE NAME AND ADDRESS Air Force Avionics Laboratory (AFAL/RWI-1) Wright-Patterson AFB, Ohio 45433		12. REPORT DATE December, 1977
		13. NUMBER OF PAGES 66
14. MONITORING AGENCY NAME & ADDRESS (if different from Controlling Office)		15. SECURITY CLASS. (of this report) Unclassified
		15a. DECLASSIFICATION/DOWNGRADING SCHEDULE
16. DISTRIBUTION STATEMENT (of this Report) Approved for public release; distribution unlimited.		
17. DISTRIBUTION STATEMENT (of the abstract entered in Block 20, if different from Report)		
18. SUPPLEMENTARY NOTES Approved for public release in accordance with AFR 190.17		<i>J. F. Guess</i> JEARAL F. GUESS, Capt, USAF Director of Information
19. KEY WORDS (Continue on reverse side if necessary and identify by block number) Atmospheric Attenuation Atmospheric Turbulence HeNe Laser		
20. ABSTRACT (Continue on reverse side if necessary and identify by block number) Atmospheric attenuation of a low-powered HeNe laser beam was examined both theoretically and experimentally. Experimental results were limited, but useful information could be extracted from the data. Close agreement was found between experimental results and theoretical predictions based on interpolation between aerosol coefficients given by McClatchey and Selby. The effects of atmospheric turbulence upon laser propagation were → next page		

Unclassified

SECURITY CLASSIFICATION OF THIS PAGE(When Data Entered)

also examined. An attempt was made to minimize the effect turbulence had upon test results, so that atmospheric attenuation could be studied independently. The conclusion of a theoretical study was that this could be accomplished by using a receiver several times larger than the beam size at the target. The prediction proved true during test runs.

The experimentation was conducted over a 1.23 kilometer course, using a 2 milliwatt HeNe laser as the transmitter, and a 12 inch spherical mirror as the receiver. Tests were conducted under visibility conditions ranging from 2 kilometers to 18 kilometers.

Unclassified

SECURITY CLASSIFICATION OF THIS PAGE(When Data Entered)